CHAPTER 8

PROPELLER CAVITATION NOISE

Cavitation of marine propellers is the most prevalent source of underwater sound in the oceans. Furthermore, when it occurs, propeller cavitation is usually the dominant noise source for any single marine vehicle. Submarines and torpedoes often operate deep enough to avoid cavitation. Surface ships, on the other hand, generally have well-developed propeller cavitation, with the result that their entire radiated spectra from as low as 5 Hz to as high as 100 kHz are controlled by this source. The basic phenomena of cavitation and cavitation noise were considered in the previous chapter. Now these concepts are combined with propeller hydrodynamics relations to explain the fundamental characteristics of propeller cavitation noise. Data on surface ship radiated noise and an analysis of the contribution of this source to low-frequency ambient ocean noise are presented in the final two sections.

8.1 Types of Propeller Cavitation

Propeller blades are rotating twisted wings that produce hydrodynamic forces. Depending on operating conditions, they experience cavitation in a number of different places, as illustrated by three typical examples shown in Fig. 8.1. Prominent in these photographs are two types of vortex cavitation: tip-vortex and hub-vortex. Propeller tip-vortex cavitation, shown most clearly in Fig. 8.1(a), is similar to wing-tip cavitation, which was discussed in Section 7.8. Hub vortices such as that shown in Fig. 8.1(c) are formed when the lift is heavy on inboard sections. Vortex cavitation produces noise, but not as much as blade-surface cavitation, which is most clearly visible in Fig. 8.1(b). In this case, the cavitation is occurring on the suction, or back, surface of the blade. When the thrust produced is small or negative, blade-surface cavitation may occur on the driving face of the blade. In addition to two types of vortex cavitation, there are two types of blade-surface cavitation: back and face. Of these, blade-surface cavitation on the suction surface is the most noisy, and hub-vortex cavitation the least.

8.2 Blade-Surface Cavitation Noise

Of the various types of cavitation, blade-surface cavitation on the suction surface produces the highest noise levels. This is because the voids collapse rapidly when they reach a region of positive collapse pressure. Both types of vortex cavitation voids, on the other hand, remain in negative pressure regions for relatively long times, tend to fill with gas as well as vapor and so collapse with less energy release.

Rotating Blade Experiments

Blade-surface cavitation can be made to occur on the surfaces of non-lifting as well as lifting

(a)

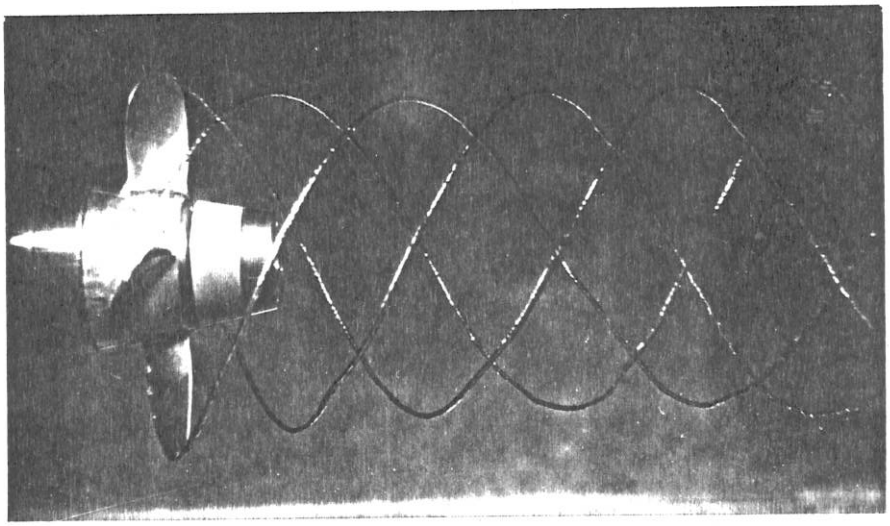

(b)

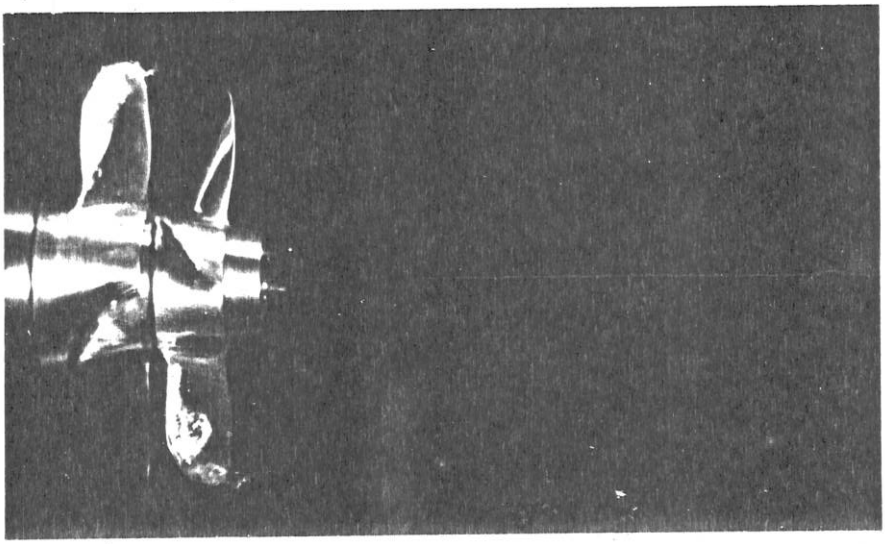

(c)

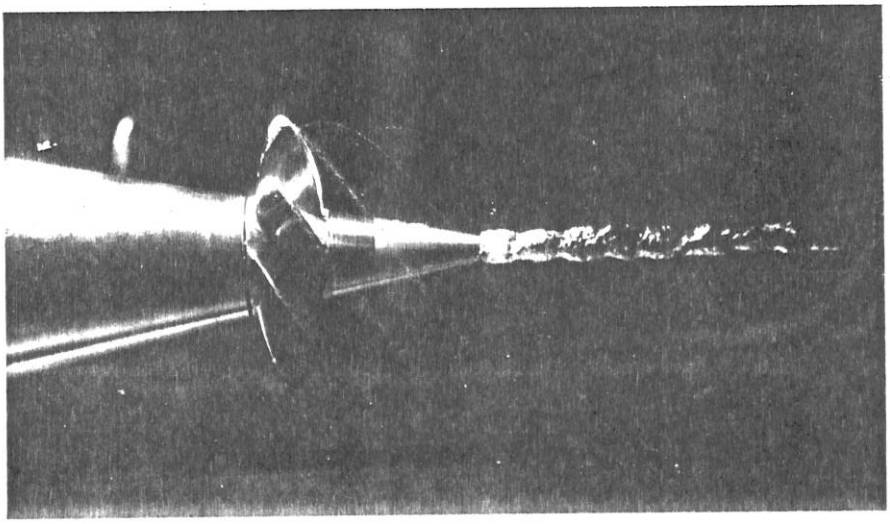

Fig. 8.1. Examples of Propeller Cavitation (Photographs taken in Garfield Thomas Water Tunnel, at The Pennsylvania State University)

blades. It can therefore be studied with an *eggbeater*-type rotating-blade apparatus in still water. Experiments of this type have been reported by Ross and McCormick (1948), Mellen (1954) and Lesunovskii and Khokha (1968). The results and analyses reported here are based on these three investigations.

Ross and McCormick reported on measurements made with an eggbeater apparatus in a lake. They measured radiated noise over the band from 17 to 60 kHz using a 1 kHz filter, finding the spectrum in this band to be continuous with a −6 dB/octave slope. As shown in Fig. 8.2, noise levels increase sharply with cavitation inception and then more gradually, even leveling off for some speed increments before resuming an upward trend. The "theoretical curves" shown in Fig. 8.2 are of the form

$$SPL = C + 10 \log \frac{N}{N_i} \left(\frac{N}{N_i} - 1 \right)^2 , \qquad (8.1)$$

which formula will be explained later in this section.

The noise measurements reported by Ross and McCormick were at frequencies above the peak of the cavitation spectrum. Measurements of a wide band including the peak were made by Mellen (1954) using a rotating rod 10 cm in diameter. As shown in Fig. 8.3, a complex triple peak was observed at about 2 kHz.

The most thorough study of blade-surface cavitation noise is that of Lesunovskii and Khokha. They studied zero-pitch airfoil-section blades having thickness-chord ratios of about 26% and diameters of 0.5 m. The critical tip index was found to be close to 1.9. Their measured spectra summarized in Figs. 8.4 and 8.5 reveal three distinctively different regimes of cavitation. The first regime, from inception to a relative speed of 1.27, is characterized by implosions of individual

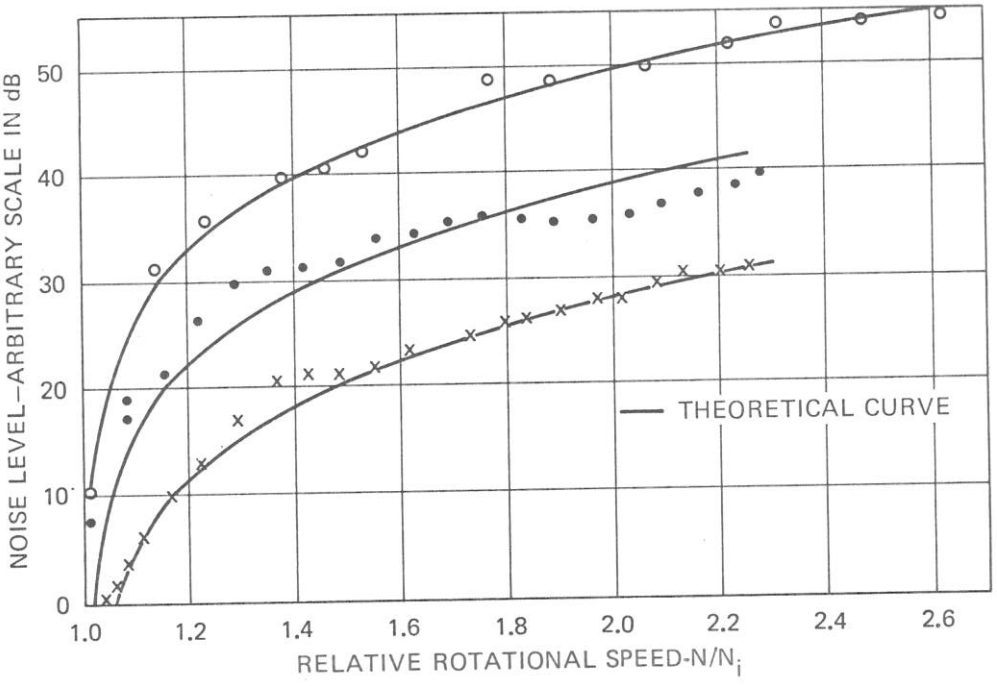

Fig. 8.2. Shape of Noise Curves for Typical Propeller Blades, after Ross and McCormick (1948)

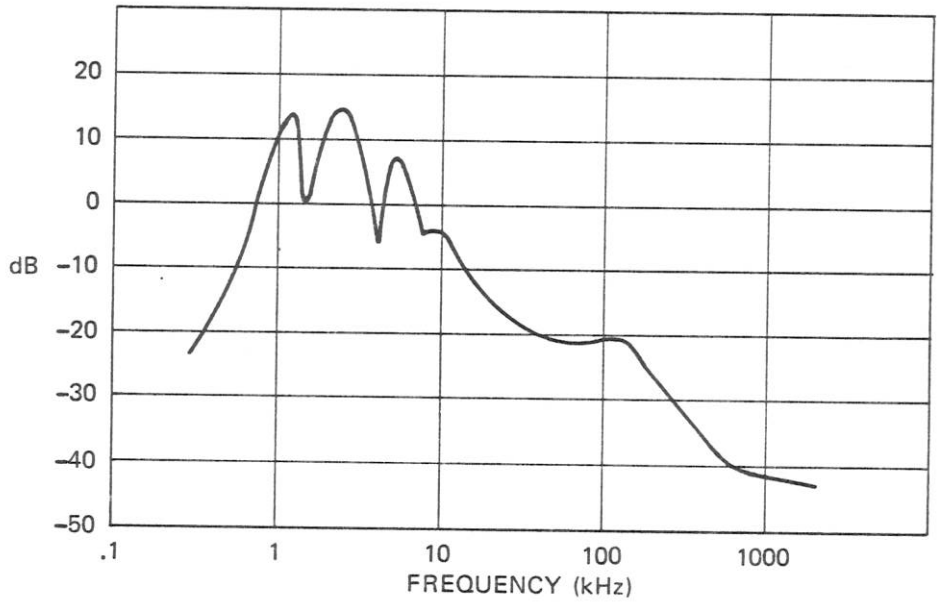

Fig. 8.3. Measured Spectrum of Cavitation Noise Using Rotating Rod, after Mellen (1954)

bubbles, called *transient cavitation*. The intensification of noise in this regime is due to increasing numbers of bubbles collapsing per second as well as increase of their size. The spectrum in this regime, corresponding to the lowest three curves in Fig. 8.4, exhibits a rounded peak. The second regime, from 1.28 to about 1.55, is characterized by a sharp spectral peak and by a peak in overall level. The sound is like a siren, the pitch of which becomes lower as the flow speed becomes greater. With a further increase in speed, the noise loses its tonality, becomes broadband and acquires a hissing character. The overall noise level rises about 15 dB in the third regime. As at lower speeds, the increase in level at low frequencies is more rapid than that at high frequencies.

Scaling Relationships

Ross and McCormick (1948) recognized that the representative local flow velocity for cavitation of a rotating blade is the tip velocity,

$$U_t = \pi n D \quad , \tag{8.2}$$

and that the appropriate flow cavitation parameter is the tip cavitation index,

$$K_t \equiv \frac{p_o - p_v}{\frac{1}{2}\rho_o U_t^2} = \frac{p_o - p_v}{\frac{1}{2}\rho_o (\pi n D)^2} \quad . \tag{8.3}$$

The blades which they used had square edges and tips and critical values of the tip index of about 2.0. A slightly lower value was measured in the Russian experiments. Values as low as 1.0 have been observed with rounded tips.

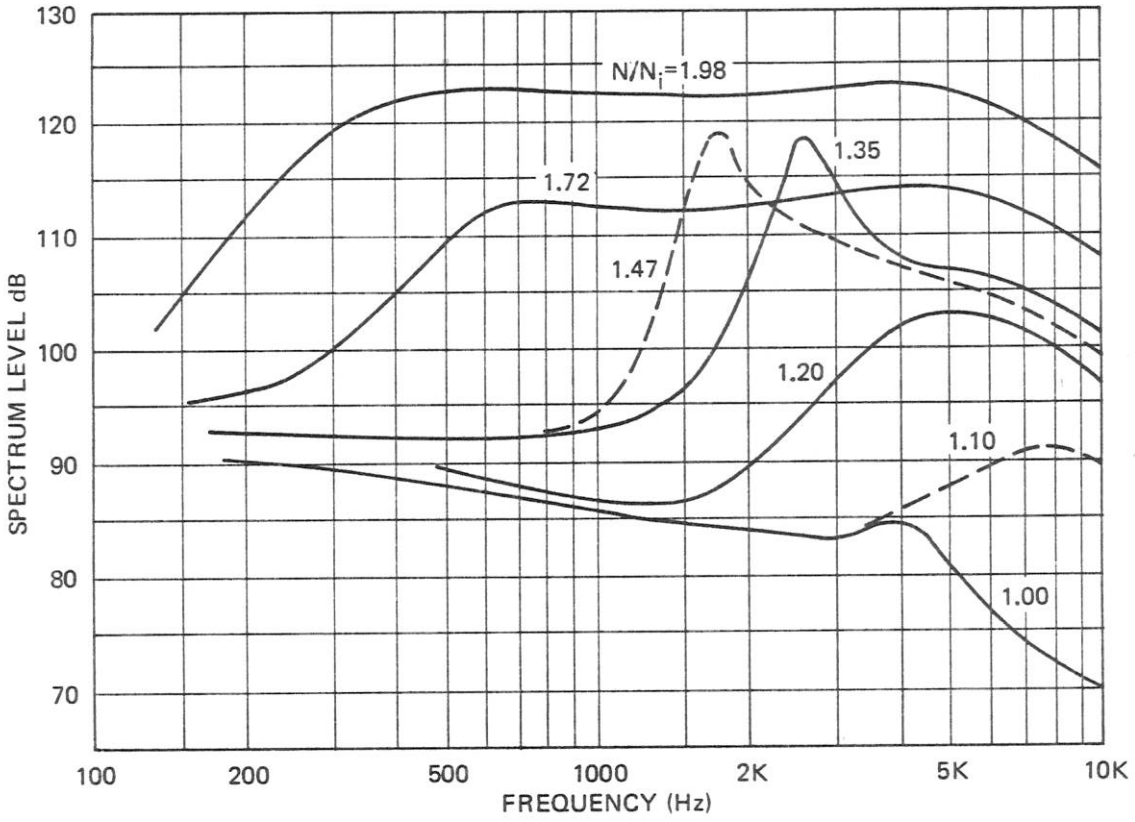

Fig. 8.4. Spectra Measured from Rotating Blades, after Lesunovskii and Khokha (1968)

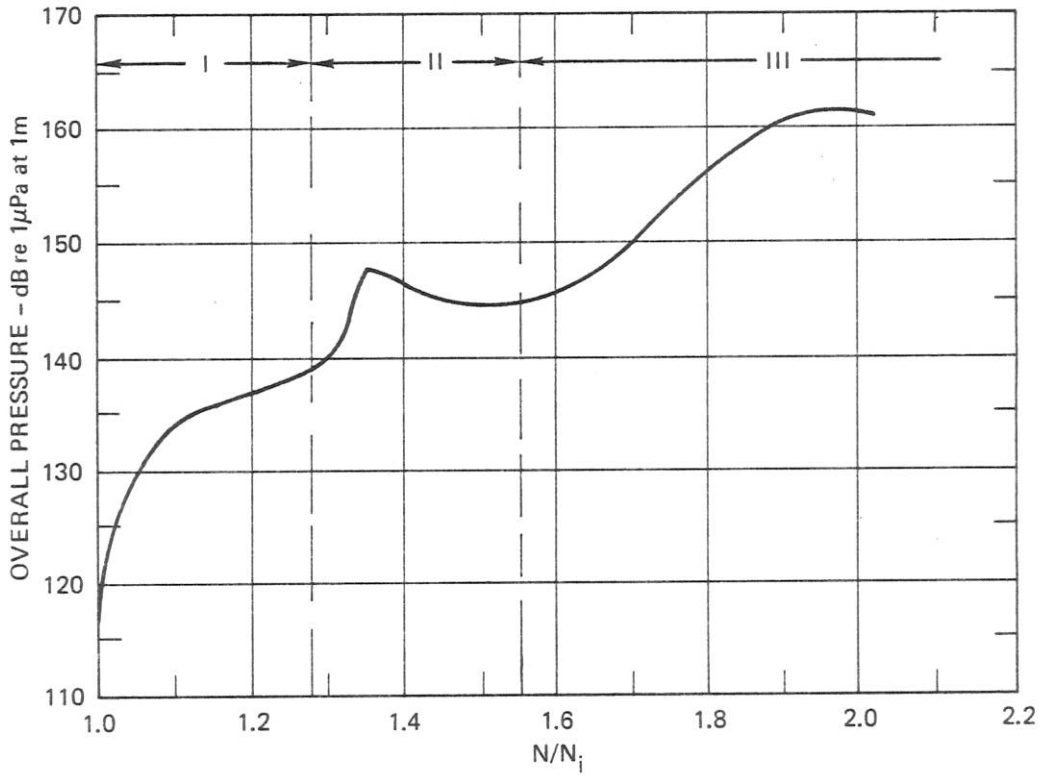

Fig. 8.5. Overall Noise Level as Function of Relative Rotational Speed, after Lesunovskii and Khokha (1968)

Ross and McCormick also developed an approximate theory for blade-surface cavitation noise scaling by means of dimensional analysis, basic physical reasoning and simplified assumptions concerning hydrofoil pressure distributions. They combined dimensional analysis with the result, described in Section 7.5, that acoustic power is proportional to the product of the collapse pressure and the volume of cavitation produced per unit time. From this synthesis they found

$$I \sim \frac{BsDPU_t}{r^2} f\left(K_t, K_{t_i}\right) , \tag{8.4}$$

where I is the total acoustic intensity, B the number of blades cavitating, s the blade chord and r the distance of the hydrophone from the source. The cavitating volume was estimated by assuming a triangular pressure distribution over the foil, whence

$$f\left(K_t, K_{t_i}\right) = \left(\sqrt{\frac{K_{t_i}}{K_t}} - 1\right)^2 = \left(\frac{U_t}{U_{t_i}} - 1\right)^2 . \tag{8.5}$$

Equation 8.4 then takes the form

$$I \sim \frac{\rho_o BsDK_{t_i} U_{t_i}^3}{r^2} \left[\left(\frac{U_t}{U_{t_i}}\right)\left(\frac{U_t}{U_{t_i}} - 1\right)^2\right] , \tag{8.6}$$

where the expression in brackets has the same speed dependence as that indicated by Eq. 8.1. When plotted on a log-log plot, Eq. 8.6 yields an average dependence on speed for well developed cavitation of about the fifth power. As we will see in Section 8.6 on merchant ship noise, this is in reasonably good agreement with trends found with full-scale ship propellers.

Equation 8.6 applies to the overall spectrum. Spectrum levels at frequencies above the spectrum peak can be estimated using a simple spectrum shape of the form

$$I_f = I_m \left(\frac{f_m}{f}\right)^2 \qquad (f \geqslant f_m) , \tag{8.7}$$

from which it follows that

$$I_f = \frac{If_m}{f^2} . \tag{8.8}$$

Peak frequency varies as the square root of pressure and inversely as the blade chord in accordance with Eq. 7.51. The frequency of the peak is also a function of the cavitation index, increasing as the index increases. From the results of Lesunovskii and Khokha, and also from some unpublished measurements on full-scale propellers, it appears that

$$f_m \sim \frac{1}{s}\sqrt{\frac{P}{\rho_o}}\, K_t^{3/2} . \tag{8.9}$$

From this it follows that the level at a given frequency varies as

$$I_f \sim \frac{BDK_{t_i} P^2}{\rho_o r^2 f^2} \left(1 - \frac{U_{t_i}}{U_t}\right)^2 , \qquad (8.10)$$

which yields a slower dependence on speed than that for the overall level, and even predicts that at high speeds high-frequency spectrum levels will remain virtually constant.

Dependence of Noise on Depth

Equation 8.10 for the high-frequency noise spectrum can be written in terms of the ratio of the operating static pressure to that for which cavitation would be suppressed at the same tip speed,

$$I_f \sim \frac{\rho_o BDK_{t_i}^{5/2} U_t^4}{r^2 f^2} p_r^2 \left(1 - \sqrt{p_r}\right)^2 , \qquad (8.11)$$

where p_r is the ratio of the actual pressure relative to that for cavitation inception. As depicted in Fig. 8.6, Eq. 8.11 predicts a maximum for high-frequency noise levels for static pressures of 30 to 60% of the inception value. For lower pressures, the noise level increases with increasing static pressure. This effect was originally observed during World War II, when it was found that high-frequency noise from submarines sometimes increased with increasing depth, rather than decreasing as was expected. The effect was named the *anomalous depth effect*. The explanation is that increased pressure causes the bubbles to collapse more rapidly and with more energy, resulting in a marked increase in peak frequency and in energy radiated at frequencies above the peak. The

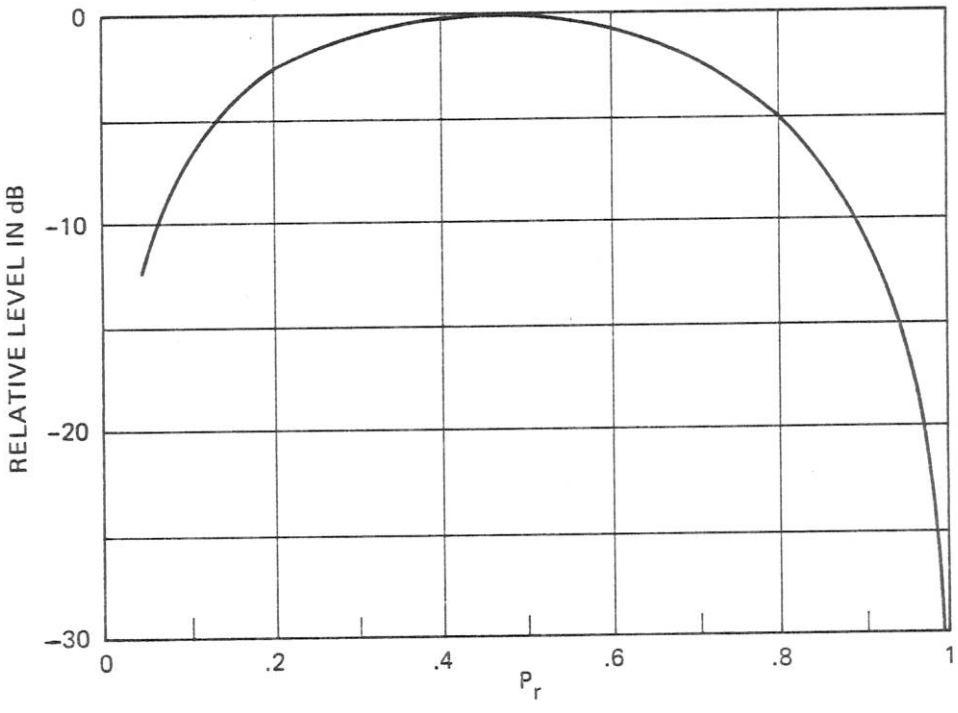

Fig. 8.6. Dependence of High-Frequency Noise on Relative Static Pressure, per Eq. 8.11

above analysis of cavitation noise provides a reasonable, though somewhat oversimplified, theoretical understanding of the anomalous depth effect and of other experimental data concerning cavitation noise.

Effect of Gas Content

The eggbeater experiment described by Ross and McCormick (1948) was carried out at a small lake over a period of more than a year. It was observed that the same amount of cavitation produced more high-frequency noise in winter months than in summer. The maximum difference was close to 10 dB. The effect was explained in terms of gas content of the water. The bottom of the lake at which the tests were run was covered with decaying vegetation, and apparently gas was released in the summer when the water was warm. The cushioning effect of the gas reduced the high-frequency noise, in accordance with the analysis presented in Section 7.4.

8.3 Propellers in Uniform Inflows

Although marine propellers operate in non-uniform turbulent wakes of vehicles, model propellers are often tested in water tunnels under uniform flow conditions. The present section on propeller operation in uniform inflows precedes discussion in the next section of the effects of flow non-uniformities.

Blade-Element Analysis

A propeller blade is essentially a twisted wing attached to a hub and can be understood in terms of aerodynamics theory. In aerodynamics, wings of finite span are usually analyzed by treating each section as a two-dimensional airfoil, the inflow velocity of which is composed of the vector sum of the flow velocity and the velocity induced by the trailing vortex system. Taking the same approach to propellers, *blade-element theory* was originally developed by Betz and Prandtl in Germany immediately after the first World War, and was further expanded by Goldstein (1929) and Theodorsen (1948).

The geometric essence of propeller blade-element analysis is illustrated by Fig. 8.7. Each differential element is formed by the intersection of a cylinder with the blade. The resultant airfoil experiences lift and drag forces due to its interaction with the inflow velocity, which is the vector sum of three components: the rotational component, $2\pi nr$; the forward speed, U_a, often called the velocity of advance; and the induced velocity, w_i, associated with the trailing vortex system. The lift and drag components of force contribute to both the thrust developed by the propeller and the torque required to keep it rotating. *Thrust* is the axial component of the resultant force,

$$dT = \cos\phi\, dF_L - \sin\phi\, dF_D \quad ; \tag{8.12}$$

torque is associated with the force components in the propeller plane,

$$dQ = r(\sin\phi\, dF_L + \cos\phi\, dF_D) \quad , \tag{8.13}$$

where angle ϕ is made by the resultant velocity vector with the propeller plane, as shown in Fig. 8.7. Both lift and drag are functions of the square of the inflow velocity and the angle of

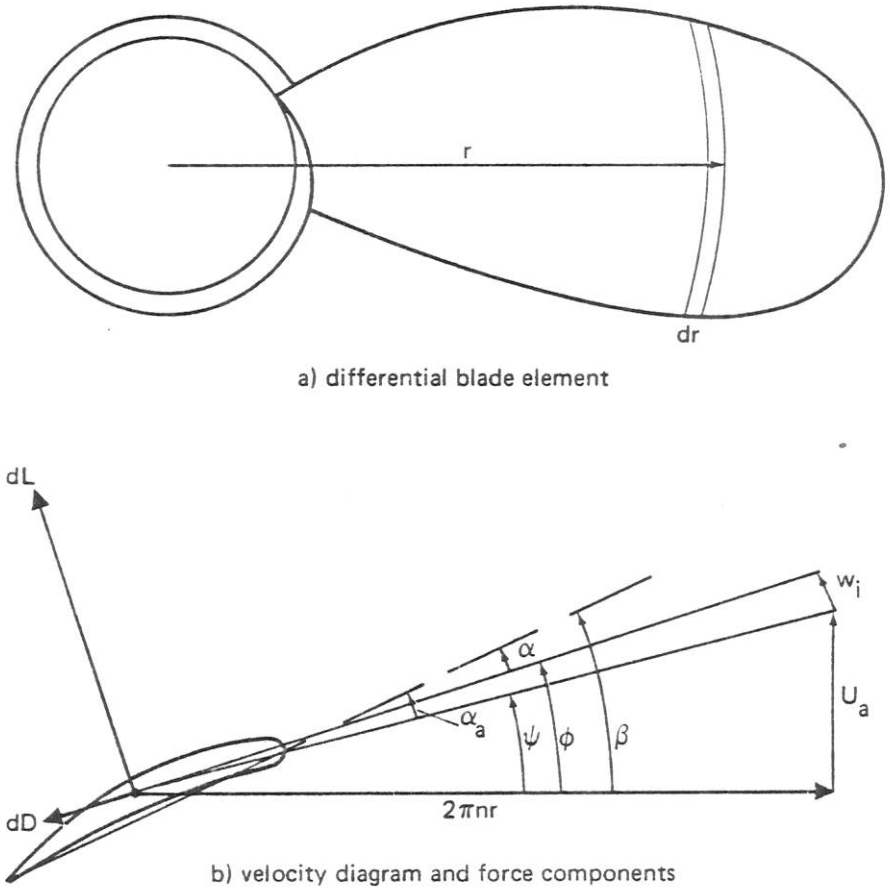

Fig. 8.7. Blade-Element Representation of a Marine Propeller

attack, α, given by

$$\alpha = \beta - \phi \ . \tag{8.14}$$

The angle β is the pitch angle of the blade-element chord. Since the induced velocity component is perpendicular to the resultant velocity, the magnitude of the inflow velocity can be estimated from the vector sum of the rotational and forward speeds,

$$U \doteq \sqrt{U_a^2 + (2\pi nr)^2} \ , \tag{8.15}$$

without actually calculating the induced velocity, w_i.

The elemental thrust and torque can be expressed in terms of the two-dimensional lift and drag coefficients of the airfoil section, given by Eqs. 7.72 and 7.73, and the magnitude of the resultant velocity, given by Eq. 8.15. The thrust is

$$dT = \frac{1}{2} \rho_o s \left(U_a^2 + (2\pi nr)^2 \right) \left(C_L \cos \phi - C_D \sin \phi \right) dr \tag{8.16}$$

and the torque is

$$dQ = \frac{1}{2}\rho_o s \left(U_a^2 + (2\pi nr)^2\right)\left(C_L \sin\phi + C_D \cos\phi\right) r dr \,. \tag{8.17}$$

The total thrust and torque are then obtained by integrating Eqs. 8.16 and 8.17 over the entire blade and multiplying by the number of blades.

The total thrust is often expressed in terms of a dimensionless *thrust coefficient*, defined by

$$C_T \equiv \frac{T}{\rho_o n^2 D^4} \,, \tag{8.18}$$

and the torque by the *torque coefficient*

$$C_Q \equiv \frac{Q}{\rho_o n^2 D^5} \,. \tag{8.19}$$

The power required to turn the propeller equals the product of the torque and the angular speed, while the useful propulsive power is the product of the thrust and the forward speed. Hence, the *propulsive efficiency* is given by

$$\eta_p = \frac{U_a}{2\pi n}\frac{T}{Q} = \frac{U_a}{2\pi nD}\frac{C_T}{C_Q} \,. \tag{8.20}$$

The ratio of the speed of advance to the rotational frequency, n, is a distance equal to that between the helical sheets that are traced out by the propeller motion. The ratio of this distance to the diameter is known as the *advance ratio*,

$$J \equiv \frac{U_a/n}{D} = \frac{U_a}{nD} \,, \tag{8.21}$$

and the *propeller efficiency* can be expressed by

$$\eta_p = \frac{J}{2\pi}\frac{C_T}{C_Q} \,. \tag{8.22}$$

Experimental measurements of propeller thrust and torque made in a water or wind tunnel are presented as plots of C_T, C_Q and η_p as functions of the advance ratio J. Figure 8.8 is typical. The efficiency peaks at an advance ratio usually about 75% of that for zero thrust.

Momentum Theory Analysis

Blade-element theory is most useful when designing a specific propeller once the diameter and advance ratio have been chosen, but it is not readily applicable to the general problem of optimum performance propellers. Momentum theory, on the other hand, can be applied to find outside limits for propeller efficiency and general relationships between efficiency and size. This theory treats a propeller as an ideal actuator disk which produces a pressure jump without frictional

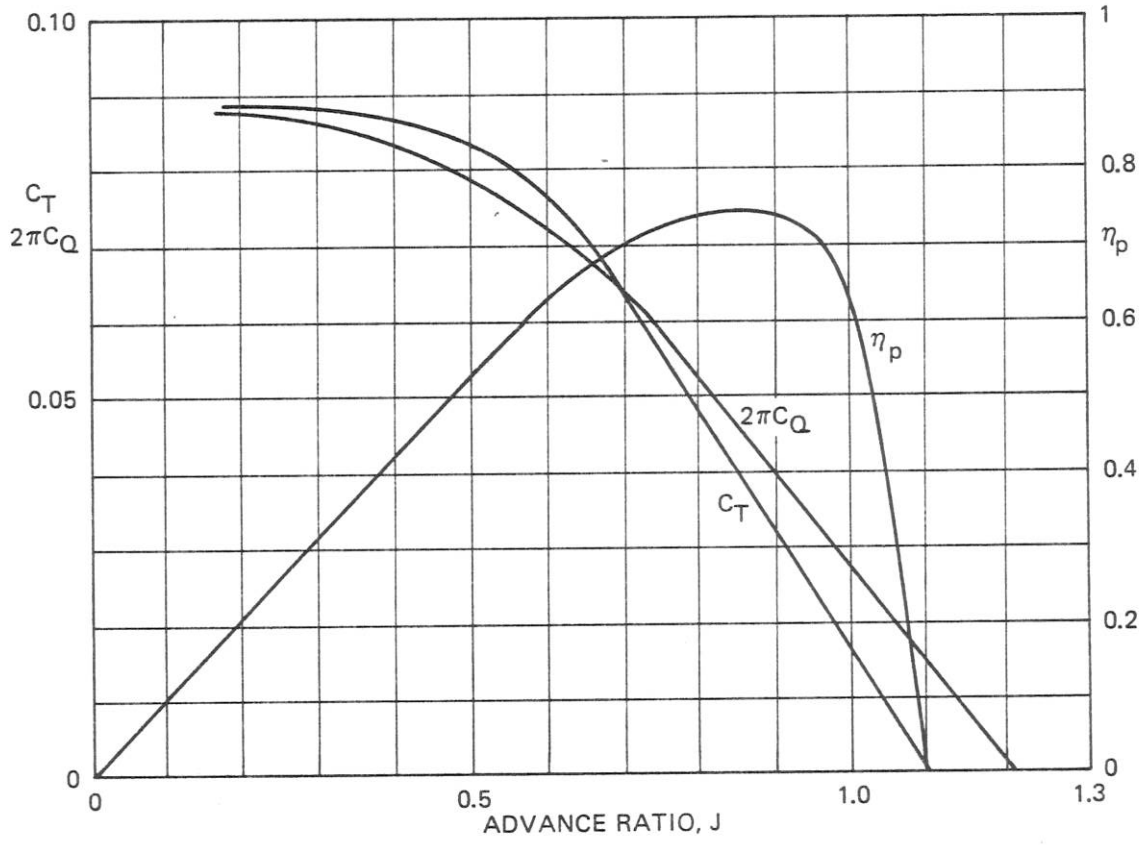

Fig. 8.8. Propeller Characteristic Curves from Open-Water Propeller Tunnel Measurements

losses. The product of the pressure jump and the propeller area equals the thrust. Associated with the pressure jump is acceleration of the flow. The rate of increase of flow energy measures the power required to drive the propeller. The smaller the pressure drop, the lower the energy; hence momentum theory predicts higher efficiencies for lightly loaded propellers. The result of application of momentum theory to this problem is a formula for the ideal, frictionless efficiency of a propeller, which may be written

$$\eta_i = \frac{2}{1 + \sqrt{1 + \tau}} , \tag{8.23}$$

where τ is the *thrust loading factor*,

$$\tau \equiv \frac{T}{\frac{1}{2} \rho_o U_a^2 S} = \frac{8}{\pi} \frac{C_T}{J^2} . \tag{8.24}$$

Equation 8.23 thus yields an expression for the ideal, frictionless efficiency as a function of thrust coefficient and advance ratio.

Momentum theory also specifies that the ideal radial distribution of thrust along the blade is that which imparts the least kinetic energy to the fluid for a given required momentum change. Under uniform inflow conditions this is achieved by uniform loading of an actuator disk. However, finite-bladed propellers impart angular momentum and energy as well as linear motion to the fluid. When this angular motion is taken into account, the optimum propeller is found to have a peak of its loading function at about 85% of the radius, with loading decreasing to zero at the tip and to near zero at the hub.

Since loading is reduced by increasing propeller diameter, momentum theory predicts higher propeller efficiencies for larger propellers. This conclusion, which has been known for many decades, has led many propeller designers to choose the maximum diameter propeller that will fit a given installation. However, it is a conclusion based on the assumption of uniform inflow conditions and, as will be seen in the next section, does not apply in radially varying wakes. Some propellers on ships are actually larger than optimum, and performance could be significantly improved by replacing them with smaller ones.

Cavitation in Uniform Inflows

The ship operator is interested in knowing propeller cavitation performance in terms of forward speed of the vessel. He therefore tends to use a cavitation parameter defined in terms of the speed of advance,

$$K_a \equiv \frac{p_o - p_v}{\frac{1}{2}\rho_o U_a^2} . \tag{8.25}$$

However, as noted above, blade-surface cavitation of rotating blades is controlled by flow speed relative to the blade tip, and a cavitation parameter defined in terms of tip speed is more meaningful. Such a *tip cavitation parameter* is defined by

$$K_t \equiv \frac{p_o - p_v}{\frac{1}{2}\rho_o U_t^2} = \frac{p_o - p_v}{\frac{1}{2}\rho_o \left(U_a^2 + (\pi nD)^2\right)} = \frac{p_o - p_v}{\frac{1}{2}\rho_o (\pi nD)^2 \left(1 + \left(\frac{J}{\pi}\right)^2\right)} , \tag{8.26}$$

which, for most practical values of J, is virtually the same as that for a rotating rod, as given by Eq. 8.3. Since the speed of advance is much smaller than the rotational component, the forward speed parameter, K_a, is always much larger than K_t. They are related by

$$K_a = \left[\left(\frac{\pi}{J}\right)^2 + 1\right] K_t . \tag{8.27}$$

It follows that for a given critical tip index the forward speed critical index can be lowered by operating at higher advance ratios, i.e., by choosing smaller diameter propellers. Thus, even for uniform inflows, cavitation considerations tend to contradict the conclusion of momentum theory by calling for smaller rather than larger diameter propellers.

Propeller cavitation inception tests are often carried out in uniform inflows in water tunnels,

the critical index being determined as a function of the advance ratio. Figure 8.9 shows typical cavitation inception characteristics plotted in terms of the tip index defined by Eq. 8.26. At high

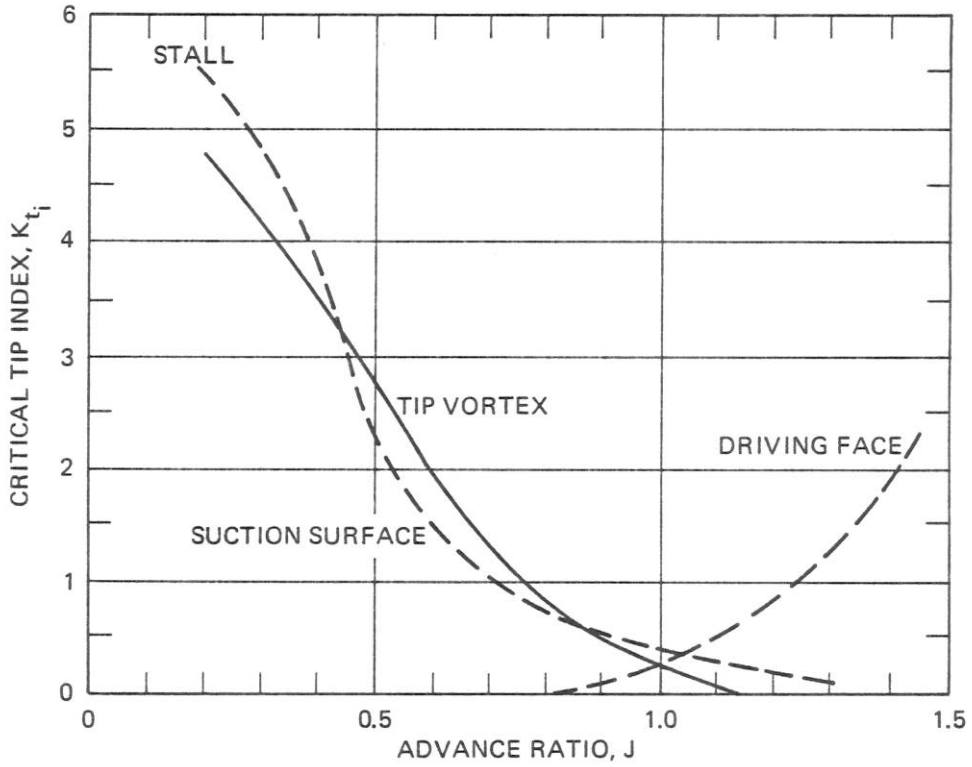

Fig. 8.9. Propeller Cavitation Inception Indices as Function of Advance Ratio in Uniform Inflow

values of the advance ratio, corresponding to small or negative values of the thrust coefficient, blade-section angles of attack are small, or negative, and driving face cavitation occurs first. As the advance ratio is decreased, and section angles of attack increased, face cavitation disappears and both suction-surface and tip-vortex cavitation become important. Finally, for very low advance ratios, angles of attack may become large enough to produce stalling, resulting in inception indices as high as 5 to 6. The optimum advance ratio for minimum inception index occurs generally at a point close to that for which efficiency is at a maximum.

Just as for hydrofoils (see Section 7.8), propellers with relatively thin blade sections achieve the lowest inception indices but are the least tolerant of operation at advance ratios differing from their design values. Thus, if a propeller is to be used in a uniform inflow environment at one specific advance ratio, thin sections are recommended, but for the more usual wake operation thicker sections are more satisfactory. In this respect, comparative tests of a number of different propellers run under uniform inflow conditions can be quite misleading when it comes to selecting the best propeller for non-uniform wake conditions.

8.4 Wake-Operating Propellers

Propeller-driven aircraft have tractor propellers operating under relatively uniform inflow conditions. By contrast, marine vehicles almost universally use pusher propellers operating in

turbulent, non-uniform wakes. There are a number of reasons for the stern placement of marine propellers, including higher propulsion efficiencies, increased dynamic stability and shorter propeller shaft lengths. The only disadvantage is operation in a non-uniform flow field and this does not outweigh the advantages.

Wake Diagrams

Inflow conditions in the plane of the propeller are illustrated by wake diagrams in which equi-velocity contours are plotted. Figure 8.10 shows such a diagram for a typical single-screw

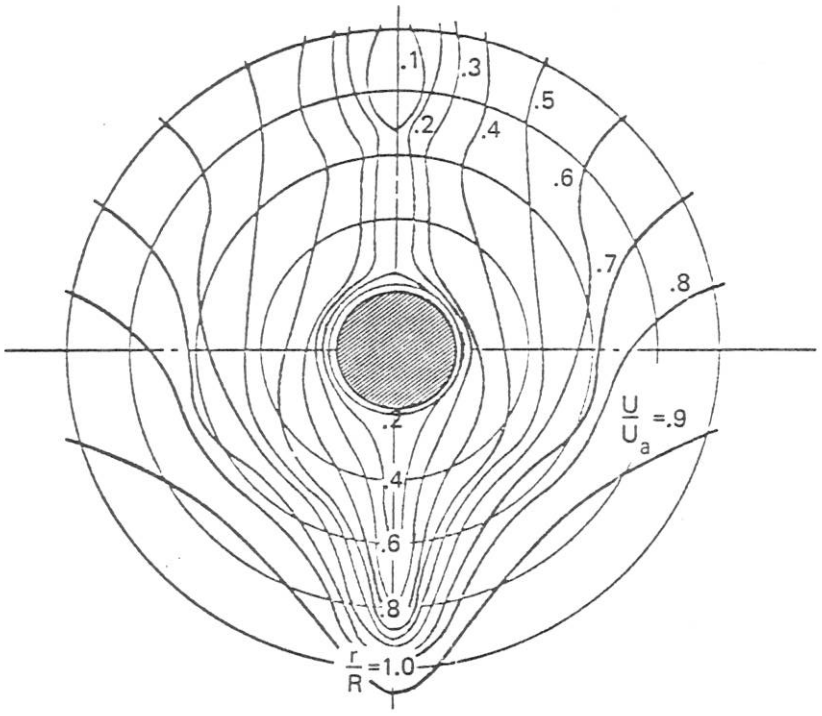

Fig. 8.10. Wake Diagram for Single-Screw Merchant Ship

merchant ship. The flow speed is seen to vary from over 90% of forward speed to less than 10%. As the propeller blade rotates, each section experiences a fluctuating inflow velocity. Figure 8.11(a) shows this variation as a function of angle, and Fig. 8.11(b) is a plot of the circumferential average velocity as a function of relative radius.

Torpedoes and many modern submarines have center-line propellers for which velocity inflows are more symmetric than for surface ships. Figure 8.12 shows a wake diagram for a typical torpedo, the only asymmetry being that caused by the four fins. While the circumferential variation is much less, the radial variation is similar to that for a merchant ship.

Operation of a propeller in a non-uniform wake differs drastically from operation in a uniform flow. Although all the effects interact, it is instructive to consider wake action as the superposition of three independent effects:

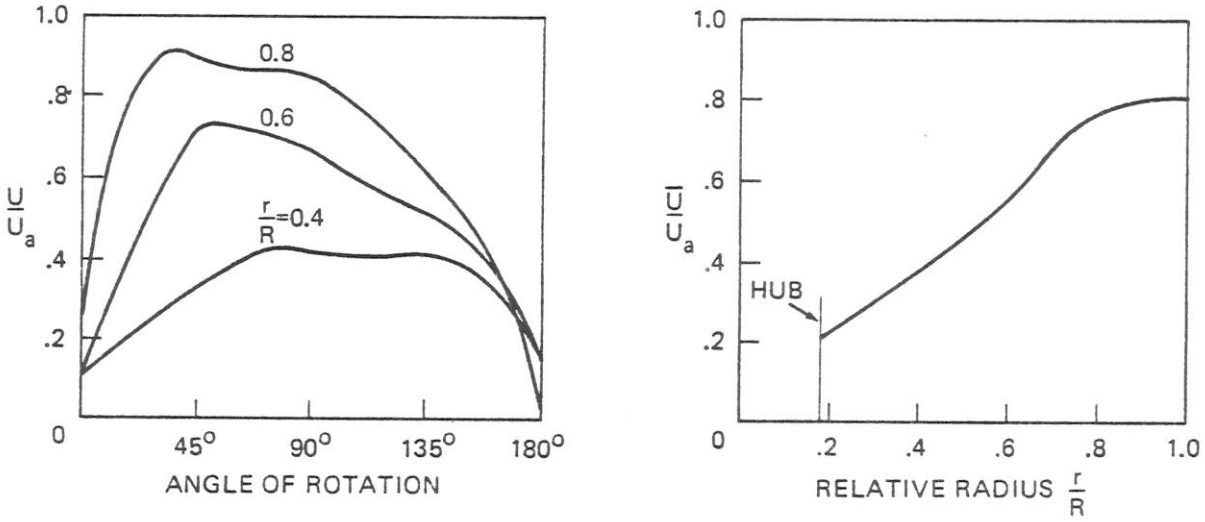

Fig. 8.11. Inflow Velocities Corresponding to Fig. 8.10

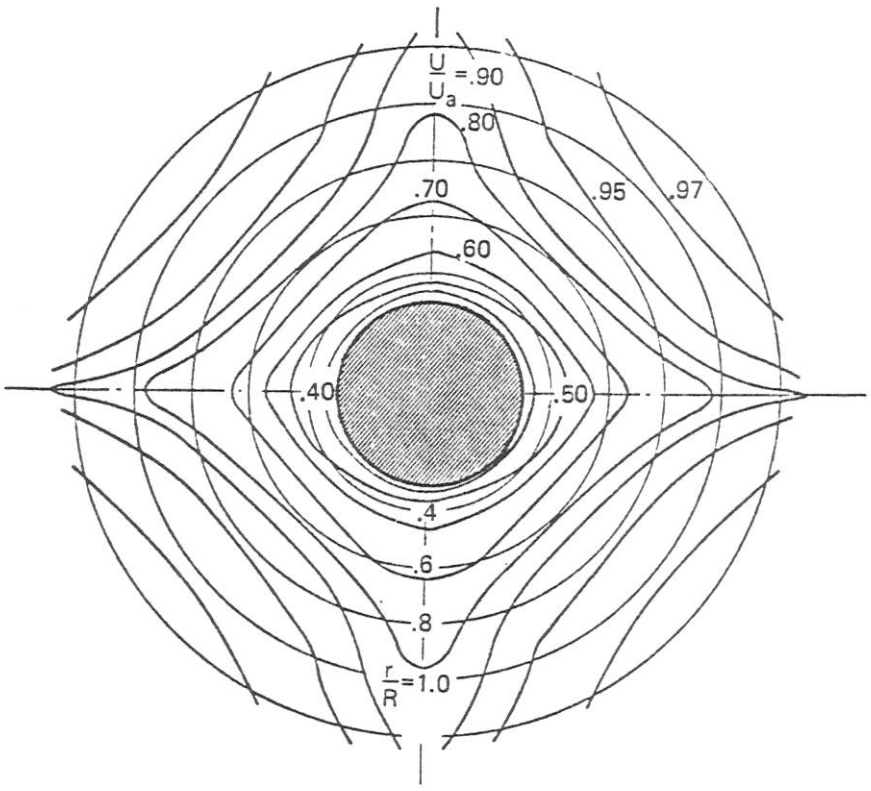

Fig. 8.12. Torpedo Wake Diagram

1) radial variation of circumferential inflow averages,
2) circumferential mean flow variations, and
3) turbulent fluctuations.

Of these, circumferential variations have by far the greatest effect on cavitation noise characteristics.

Effect of Radially Varying Inflow

The most obvious effect of a radially varying inflow is to alter velocity vectors of the inboard sections. Instead of the effective advance velocity being U_a, as in Fig. 8.7, it is the local circumferential average, as shown in Fig. 8.11(b). The effect on the magnitude of the resultant inflow velocity is small, since the rotational component is relatively large. By far the more important effect is to change the angle of attack.

Propeller designers have long recognized the effect of a radial wake on section angles of attack; not until the mid 1940's was it also realized that optimum load distributions are different. Application of momentum theory to wake operation leads to the conclusion that the optimum actuator-disk propeller is the one that tends to fill in the momentum deficiency of the wake. Such a propeller would be heavily loaded in its inboard sections and virtually unloaded near the blade tips. Its diameter would equal that of the wake. Lane (1952) applied the Betz-Prandtl blade-element theory to wake-operating finite-bladed propellers much as Goldstein had applied it to propellers in uniform flows. He confirmed that the optimum loading function is shifted toward the inboard sections, and that an optimum wake-operating propeller has a smaller diameter than one designed for uniform conditions. Propellers embodying these principles have been designed for torpedoes at the Garfield Thomas Water Tunnel at the Pennsylvania State University. As shown in Fig. 8.13, they have a large number of relatively stubby blades.

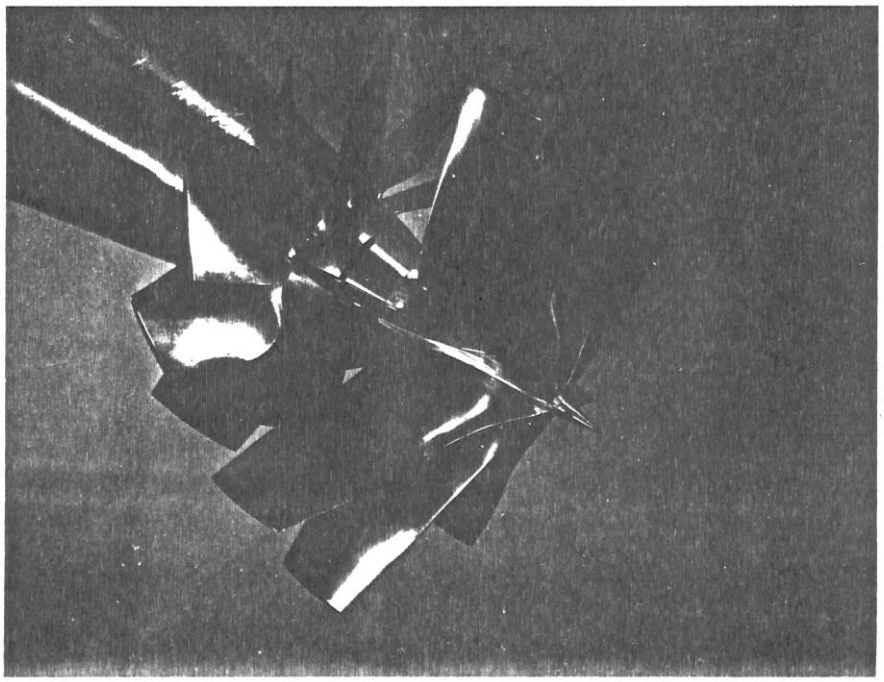

Fig. 8.13. Modern Torpedo Propeller Designed for Radially Varying Inflow, courtesy Garfield Thomas Water Tunnel

While design for a radial wake tends to reduce susceptibility to blade-surface and tip-vortex cavitation by unloading the tip sections, the shift to high inboard loading increases the strength of the hub vortex. In early designs the trend was carried too far, creating a strong hub vortex that not only cavitated prematurely but also caused a reduction of overall propulsive efficiency due to the accompanying severe pressure drop at the center of the tail cone. Later designs have compromised between dictates of momentum theory and the necessity of limiting hub vorticity.

Effects of Circumferential Variations

It is circumferential wake variations that are responsible for most of the deleterious effects of wake operation. As discussed above, variations of inflow velocity cause large variations of angle of attack. As a result of these variations, each blade element produces a varying amount of lift, resulting in significant fluctuations of thrust and torque during each revolution of the propeller. Oscillating components as high as 10% of average values are quite typical for single-screw merchant ships. It is these oscillating components which shake the hull and cause severe vibration. Such fluctuating forces also produce tonal sound radiation, as will be discussed in Chapter 9.

Effect on Cavitation

Compared to operation in uniform inflows, wake operation causes dramatic increase of critical inception indices and strong amplitude modulation of cavitation noise spectra. The effect of operating in a circumferentially varying wake is similar to, though not exactly equivalent to, operating a propeller with variable advance ratio. As shown in Fig. 8.9, the inception index is a strong function of the advance ratio. The index for a wake-operating propeller may equal that for the most extreme operating condition occurring as the blade rotates.

Consider the propeller whose uniform inflow characteristics are represented by Figs. 8.8 and 8.9. This propeller is designed to operate at a nominal advance ratio, J, of about 0.9, for which its critical tip cavitation index is about 0.5. When operating in a ship's wake, the swings in blade angle of attack may be equivalent to operation between J's of 0.4 and 1.2, and the critical inception index may then be as high as 3.5 to 4. If the operating cavitation parameter were 2, each blade would be free of cavitation at all times except for the very short period when the angles of attack were equivalent to operation at $J < 0.6$. The resultant burst of cavitation noise would be very short-lived, sounding like a high-pitched click. Since one blade invariably cavitates sooner than the others, the bursts would first occur once per revolution. As the other blades join, the bursts would become more frequent, finally occurring at *blade rate*, i.e., the number of blades times rotational frequency. If the speed were increased and the cavitation index lowered still further, the point would be reached where cavitation noise would be continuous, since at least one blade would be cavitating at all times. However, the resultant spectrum would be strongly modulated at blade-rate frequency. Since, as mentioned above, one blade invariably cavitates more than the others, there is also a superimposed shaft-rate modulation. It is this shaft-rate modulation that can be detected by the human ear and which enables an experienced sonar operator to determine the propeller rpm and thereby often classify the target.

The effect of wake operation on cavitation inception is so dramatic that the critical inception index usually depends more on the wake than on the design of the propeller. Thus, for severe wakes, such as that shown in Fig. 8.10, stall is likely to occur when the blade passes behind the stern post. At this point one would expect a critical index of 3 to 6 independent of propeller design. On the other hand, critical indices of 1 to 2 are common for moderate wakes such as that of Fig. 8.12. Only under practically uniform flow conditions will values below 1 be achieved.

These generalizations are summarized in Fig. 8.14, which can be used to predict the likelihood of propeller cavitation based merely on the tip cavitation parameter, K_t, and a general evaluation of the nature of the wake.

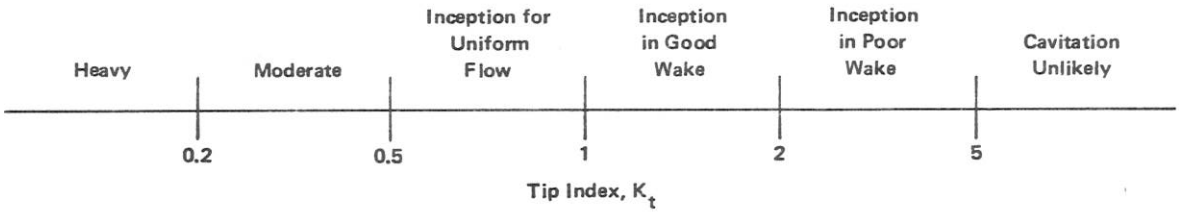

Fig. 8.14. Qualitative Cavitation Relationships to Tip Index

Low-Frequency Cavitation Tonals

As reported by Aleksandrov (1962), low-frequency spectra of cavitating ship propellers are usually dominated by tonal components at harmonics of the rotational frequency, blade-rate harmonics being strongest. Since ship propellers generally operate at from 60 to 350 rpm and have from three to six blades, the fundamental repetition frequencies of this type of sound vary from 1 to 18 Hz. The strongest components are generally harmonics between 10 and 70 Hz. This direct radiation of tones occurs at the same frequencies as modulation of the cavitation continuum, and Aleksandrov attributed it to radiation by the aggregate of cavitation bubbles. If one considers the total void volume of cavitation bubbles on a blade at any one time to act as a single volume, then fluctuations of this volume caused by operation at varying angles of attack can be expected to radiate sound directly by the monopole mechanism described in Chapter 4 for pulsating bubbles.

It is now clear why cavitation is such a dominant noise source. Not only does collapse of many individual bubbles produce a continuous spectrum that extends from as low as 50 or 100 Hz to over 50 kHz, but also pulsations of the aggregate volume of cavitation radiate strong tonals at frequencies below 70 Hz.

8.5 Submarine Propeller Cavitation

During World War II passive sonars were used to detect submarines at frequencies above 1 kHz, often above 10 kHz. At these frequencies submarines were virtually undetectable when not cavitating and easily detectable when cavitating. Differences in noise levels between the two conditions were greater than 40 dB. Although cavitation inception was recognized as the limit to quiet operation, inception speeds at periscope depth were generally as low as 3 to 5 kts.

One reason for the poor cavitation performance of submarines was that their propellers had been designed for and tested in uniform inflow conditions. Submarines in WWII had twin screws and propeller diameters were the largest that would just miss scraping the hull. Consequently, tip sections passed through the region of the hull boundary layer where flow velocities were very low. The resultant angles of attack were high enough to cause local blade stall and consequent high inception cavitation indices.

Figure 8.15 shows typical noise data for WWII submarines plotted as a function of speed in m/sec divided by the square root of effective depth, given by the actual depth plus 9 m. Since

cavitation of submarine propellers occurs when the tips are passing through a region of low forward speed, the appropriate tip cavitation index is that for rotating rods given by Eq. 8.3. This can be expressed in terms of the depth of submergence by

$$K_t \doteq \frac{2}{3} \frac{h + 9}{\left(\frac{N}{100}\right)^2 D^2} , \tag{8.28}$$

where h is the depth of the propeller tip below the surface in meters, D is the propeller diameter in meters and N is the rotational speed in rpm.* Utilizing Eq. 8.21 for the advance ratio, K_t can also be expressed in terms of the forward speed by

$$K_t \doteq 1.85 \frac{h + 9}{U_a^2} J^2 , \tag{8.29}$$

where U_a is in m/sec.* For the submarines represented in Fig. 8.15, $J \doteq 0.8$ and the critical

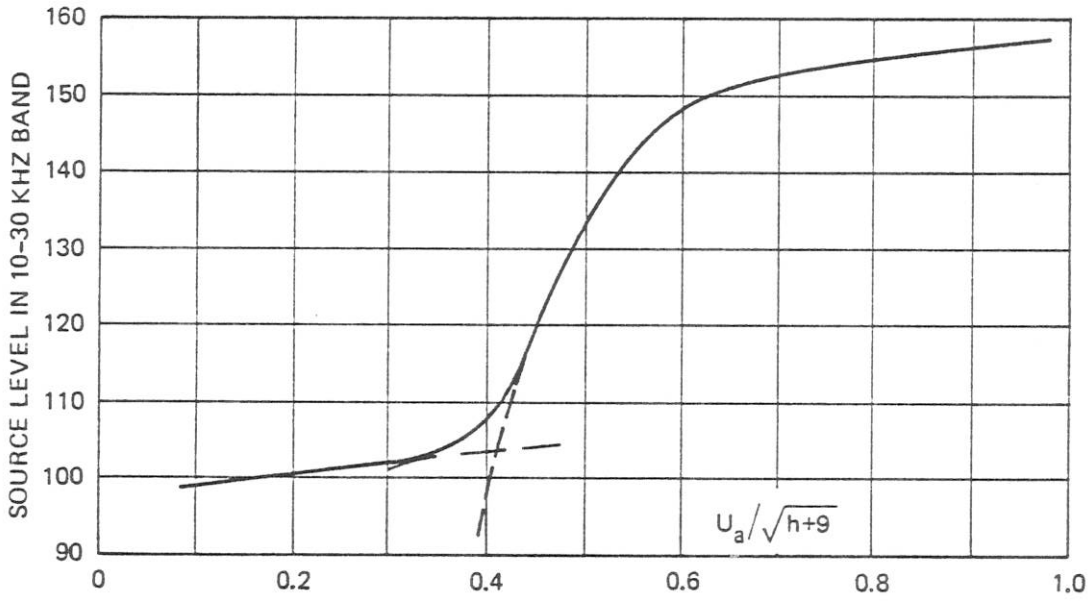

Fig. 8.15. High-Frequency Noise of World War II U.S. Submarines, as Measured by Strasberg and Sette (1944)

*For readers who are more at home with English units, Eq. 8.28 can be written:

$$K_t \doteq 2.2 \frac{h + 30}{\left(\frac{N}{100}\right)^2 D^2} , \tag{8.28a}$$

where both h and D are measured in feet. When U_a is expressed in kts and h in ft, Eq. 8.29 becomes

$$K_t \doteq 2.1 \frac{h + 30}{U_a^2} J^2 . \tag{8.29a}$$

inception value of the speed/$\sqrt{\text{depth}}$ ratio of 0.4 corresponds to a tip index of about 6. Model tests of submarine propellers in uniform inflows corresponding to mean flow conditions predicted cavitation inception at speeds two to three times those actually observed. On the other hand, tests of a submarine propeller in still water, corresponding to boundary-layer operation, yielded an inception tip index of 6, confirming that cavitation was indeed controlled by the most extreme part of the wake.

Following WWII, in converting WWII Fleet submarines to modernized Guppy types, propeller diameters were reduced, and a significant increase in the speed for cavitation inception was achieved. Nuclear submarines have entirely different tail configurations and many have single center-line screws. Cavitation inception speeds of these submarines are therefore much higher than those that were typical during WWII.

Figure 8.16 shows several typical submarine cavitation spectra measured during WWII in which it is seen that the peak moves to lower frequencies as speed increases, as would be expected from the discussion of cavitation spectra in Section 7.5. The *anomalous depth effect* discussed in Section 8.2 and predicted by Eq. 8.11 is confirmed by measurements of submarine noise as a function of depth shown in Fig. 8.17.

8.6 Surface Ship Radiated Noise

Importance of Propeller Cavitation

Radiated spectra of surface ships are dominated by propeller cavitation noise except when the ships are operating at very slow speeds. This is readily confirmed by calculating the operating tip-cavitation parameter from Eq. 8.28. A typical merchant ship having a length of about 200 m may have a 7 m diameter propeller operating at about 100 rpm, yielding a tip index of the order of

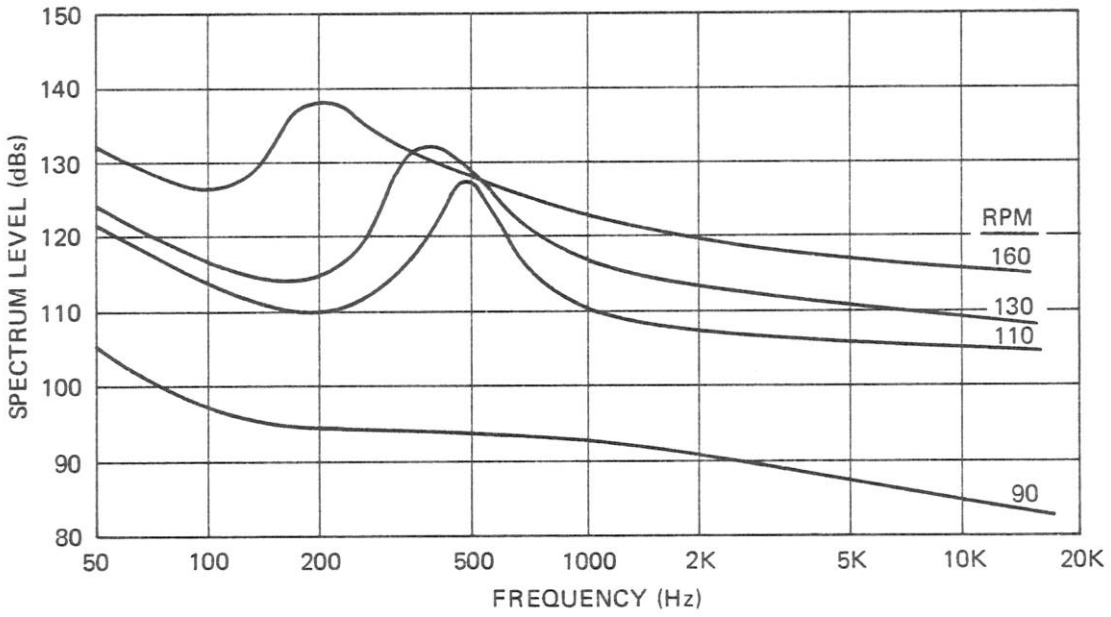

Fig. 8.16. Measured Submarine Cavitation Spectra, after Strasberg and Sette (1944)

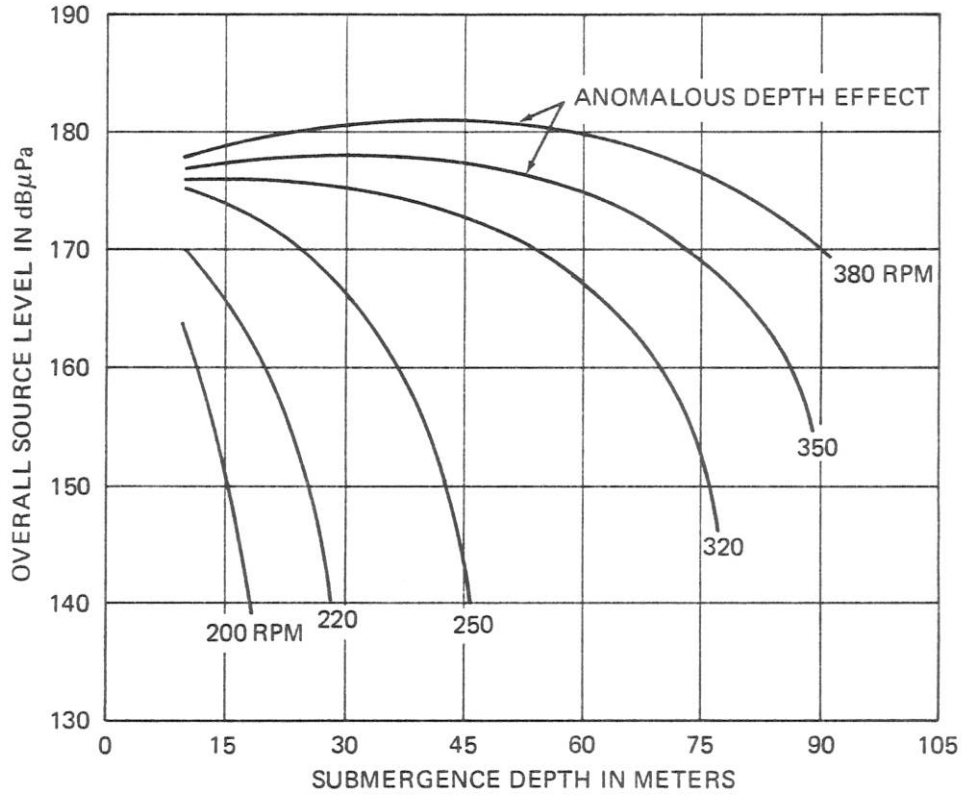

Fig. 8.17. Effect of Depth on WWII Submarine Propeller Cavitation Noise

0.2, close to a factor of 20 lower than the likely inception value of 3 to 4. Thus, a merchant ship near its normal cruise speed usually operates at a speed about four times that for which the first traces of cavitation occur.

The statement made here that merchant ships operate at speeds as much as four times cavitation inception speed is at variance with the claim usually made by naval architects that this ratio is less than two. Naval architects are concerned with the effects of cavitation on performance and usually quote inception speeds based on open-water tests, for which the inception tip index would be less than 1. However, when treating radiated noise characteristics the pertinent inception speed is that for which the first traces of cavitation occur as blades pass behind the stern post. As discussed in Section 8.4, the tip index is almost always higher than 3 for surface ships having asymmetrical wakes of the type shown in Fig. 8.10.

Other characteristics of surface ship noise that confirm the dominance of propeller cavitation are strong modulation of the broadband spectrum at shaft and blade frequencies and the radiation of low-frequency tonals at harmonics of these frequencies. These features are discussed later in the present section.

World War II Noise Data

The only sources of extensive data on surface ship radiated noise spectra are measurements made during WWII, reported in a compendium issued by the U.S. Office of Scientific Research and Development (O.S.R.D.) in 1945 and declassified in 1960. Measurements were made on American,

Canadian and British ranges. Results reported for a British cruiser and passenger vessel are presented in Figs. 8.18 and 8.19. Measurements were made on the botton in 40 m deep water at Innellan, Scotland. The data have been converted into source levels at 1 m relative to 1 μPa by a process which may introduce errors of up to 3 dB.

Many of the surface ships ranged in the early 1940's showed the following typical trends:

a) sound in the mid-frequency range of 500 to 1000 Hz increases as U^5 to U^6,

b) the spectral slope is about -5.5 to -6 dB/octave at the higher speeds and as much as -7 to -8 dB/octave at low speeds, and

c) the rate of increase with speed is greater for frequencies below 100 Hz.

For ships proceeding at near cruise speeds. WWII results for frequencies over 100 Hz can be written

$$L_s = L'_S + 20 - 20 \log f \qquad (f \geqslant 100) \ , \tag{8.30}$$

where f is frequency in Hz and L'_S is the overall level measured in the band from 100 Hz to 10 kHz. Spectra below 100 Hz are quite variable, as indicated by Figs. 8.18 and 8.19. Near cruise speed, the radiated power below 100 Hz usually exceeds that above 100 Hz by from 2 to 8 dB. Figure 8.20 represents the average surface ship spectrum plotted relative to overall level in the band above 100 Hz, i.e., in dBs relative to L'_S. Shown in this figure along with the average

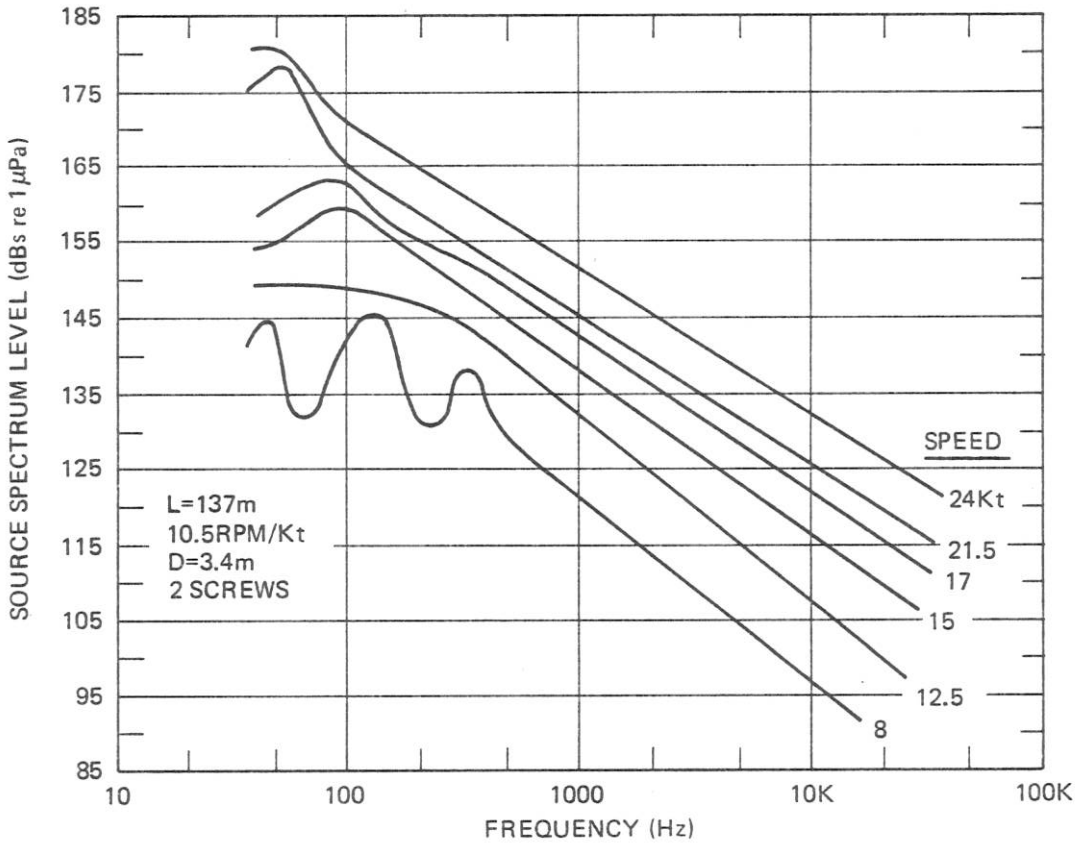

Fig. 8.18. Radiated Noise of British Cruiser *Cardiff*, as Measured in WWII

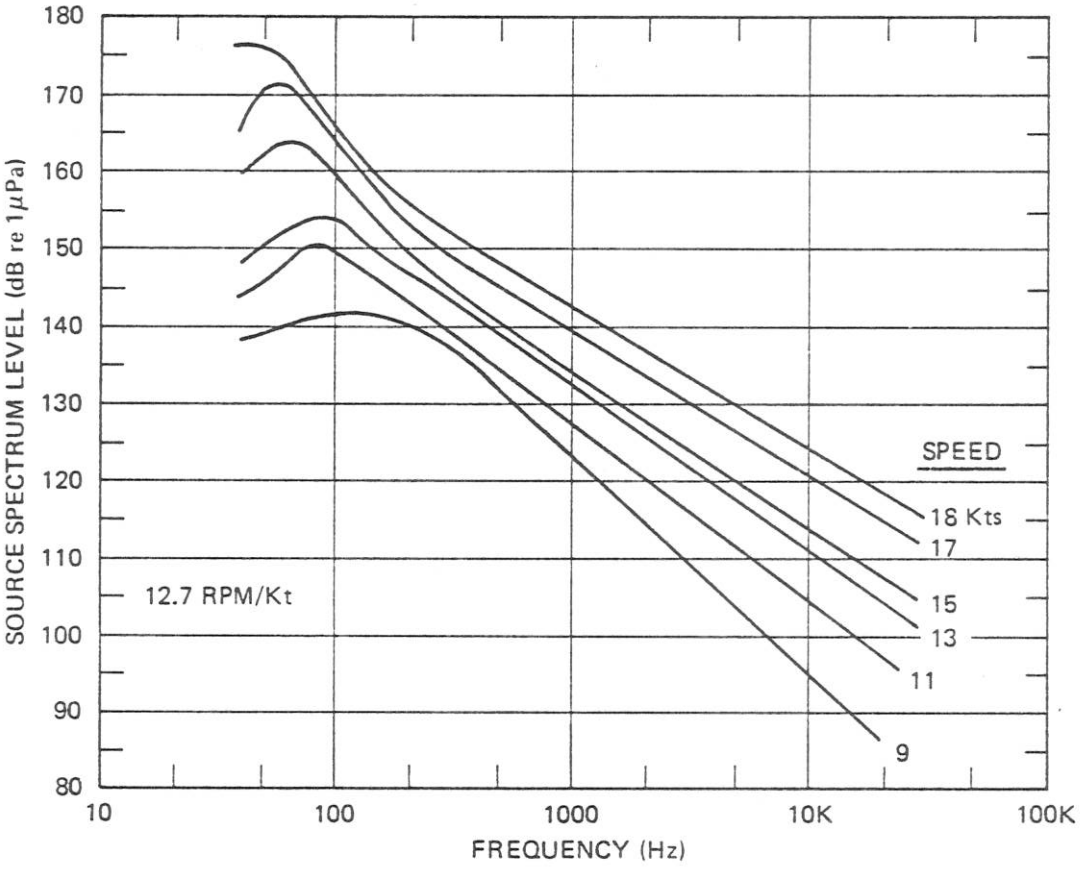

Fig. 8.19. Radiated Noise of Passenger Ship *Astrid*, as Measured during WWII

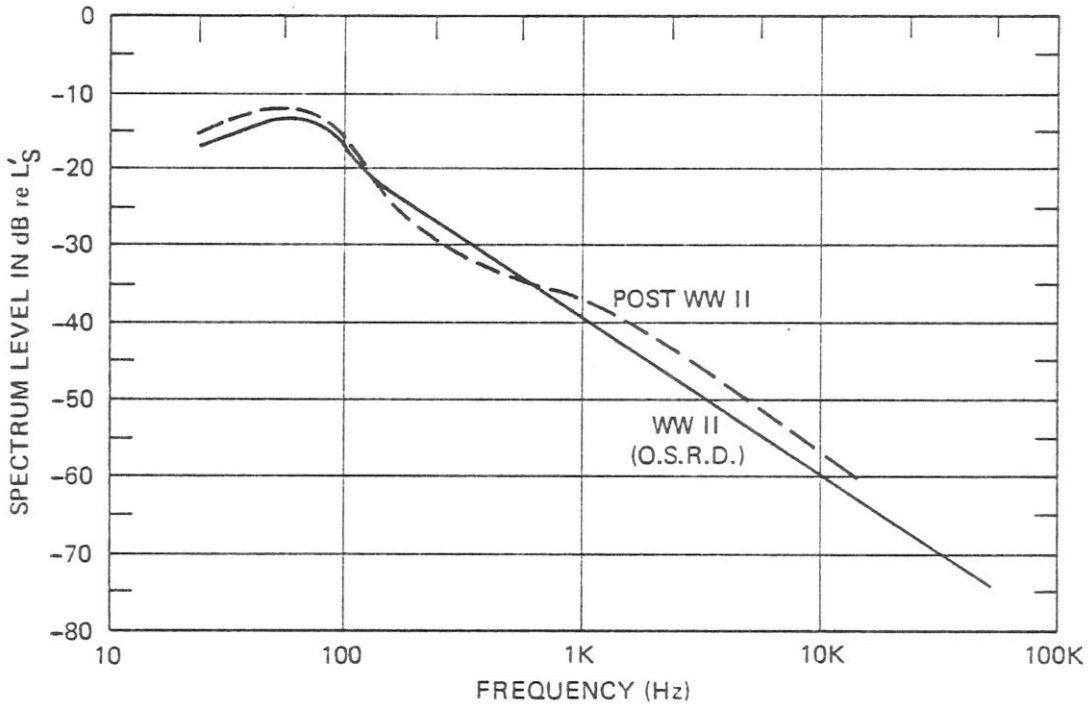

Fig. 8.20. Average Relative Spectra of Surface Ships

spectrum from WWII is the average curve from a number of post-war measurements of freighters and tankers which shows more structure than the WWII average and deviates from Eq. 8.30 by from 1 to 3 dB over much of the spectrum.

Dependence on Speed

Many measurements made during WWII were at speeds that are about half those of modern ships, although a few measurements of naval ships extended beyond 15 kts. Figure 8.21 summarizes data on speed dependence of the overall level, L'_S, for measurements of ships from 8 to 24 kts. The trend curve that has been drawn through the data fits the equation

$$L'_S = 170 + 53 \log \frac{U_a}{10\ kt}\ , \tag{8.31}$$

where 10 kts is taken as the reference speed, or

$$L'_S = 179 + 53 \log \frac{U_a}{15\ kt} \tag{8.32}$$

in terms of the level at 15 kts. Average values for several ships vary by ±4 dB from the trend curve.

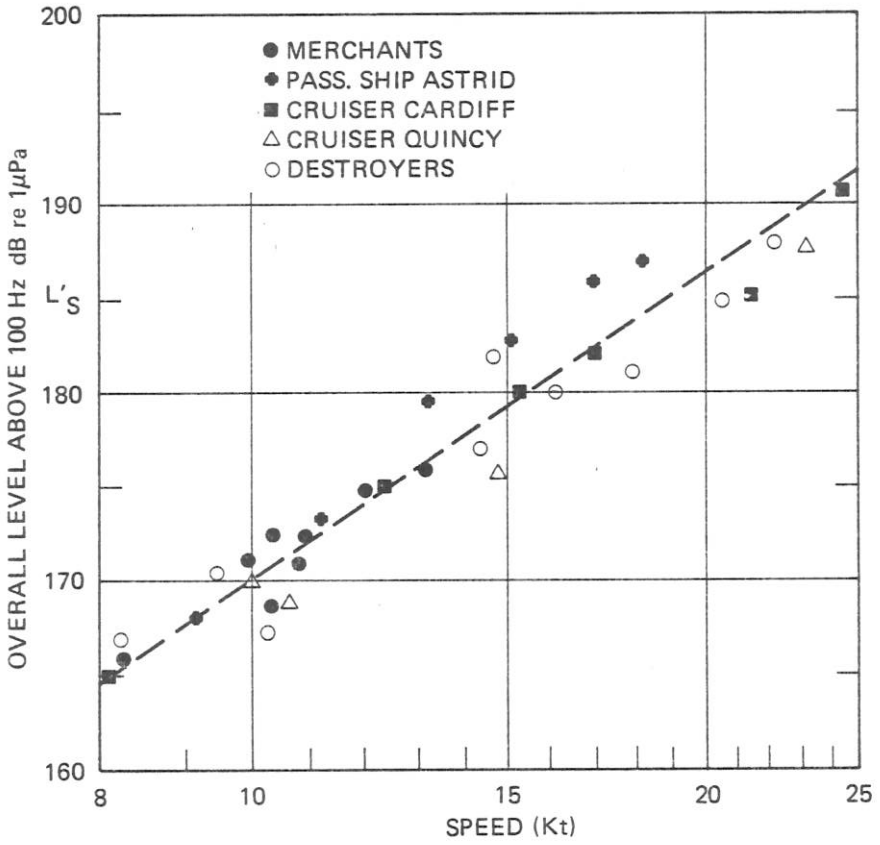

Fig. 8.21. Speed Dependence of Overall Radiated Level of Surface Ships, as Measured during WWII

Estimation Formulas

The trends shown in Fig. 8.21 and represented by Eqs. 8.31 and 8.32 are somewhat contaminated by the fact that faster ships are generally larger than slower ones. Thus, the two factors of size and speed are both involved in the trend curve. That size is important was revealed by WWII data on battleships and aircraft carriers, which invariably were found to be about 10 dB noisier than smaller ships at the same speeds. Several formulas using tonnage as an indicator of size were developed during WWII. Two of the more popular ones may be expressed in terms of overall level above 100 Hz, L'_S, by

$$L'_S \doteq 112 + 50 \log \frac{U_a}{10\ kt} + 15 \log DT \tag{8.33}$$

and

$$L'_S \doteq 134 + 60 \log \frac{U_a}{10\ kt} + 9 \log DT\ , \tag{8.34}$$

where DT is the displacement tonnage. These two formulas give similar results for ships of the types at sea in WWII. However, some modern supertankers are more than 20 times as large and the differences between levels predicted by the two formulas can be as much 10 dB for ships of this size. For this reason the author recommends that these formulas not be used for ships of over 30,000 tons.

Formulas developed in Section 8.2 for blade-surface cavitation noise indicate that propeller cavitation noise power should be proportional to total number of blades cavitating and to propeller diameter, and is a function of tip speed, the dependence on tip speed being strongest. Ship size or tonnage would not be expected to enter the equation except to the extent that the product of number of blades and diameter is usually bigger for larger ships. When data from WWII are examined, there is found to be a clear trend with tip speed and number of blades and none with any other variable. Noise data for ships over 100 m length can be represented by

$$L'_S \doteq 175 + 60 \log \frac{U_t}{25\ m/s} + 10 \log \frac{B}{4} \tag{8.35}$$

over the range of tip speeds from about 15 to 50 m/sec.* The apparent trends with tonnage that were expressed in Eqs. 8.33 and 8.34 are now attributable to the fact that heavier vessels usually require higher propeller loading, i.e., higher values of tip speed per knot and more blades. Equations 8.31, 8.32 and 8.35 yield similar levels for four-bladed propellers having advance ratios

*With U_t expressed in ft/sec, Eq. 8.35 becomes:

$$L'_S \doteq 180 + 60 \log \frac{U_t}{100\ fps} + 10 \log \frac{B}{4}\ , \tag{8.35a}$$

where L'_S is the overall level above 100 Hz in dB relative to 1 μPa at a reference distance of 1 yd.

of the order of 0.85. For ship propellers with lower advance ratios, Eqs. 8.31 and 8.32 may be expected to underestimate the noise radiated. Thus, data from battleships and aircraft carriers are better represented by Eq. 8.35 than by Eqs. 8.31 and 8.32. Their relatively high levels are partly explained by the large number of blades cavitating (8 to 12) and by operation at advance ratios lower than 0.85. Figure 8.22 is a plot of overall noise as a function of tip speed, as given by Eq. 8.35. Individual ships can be expected to differ from the curve by ±5 dB.

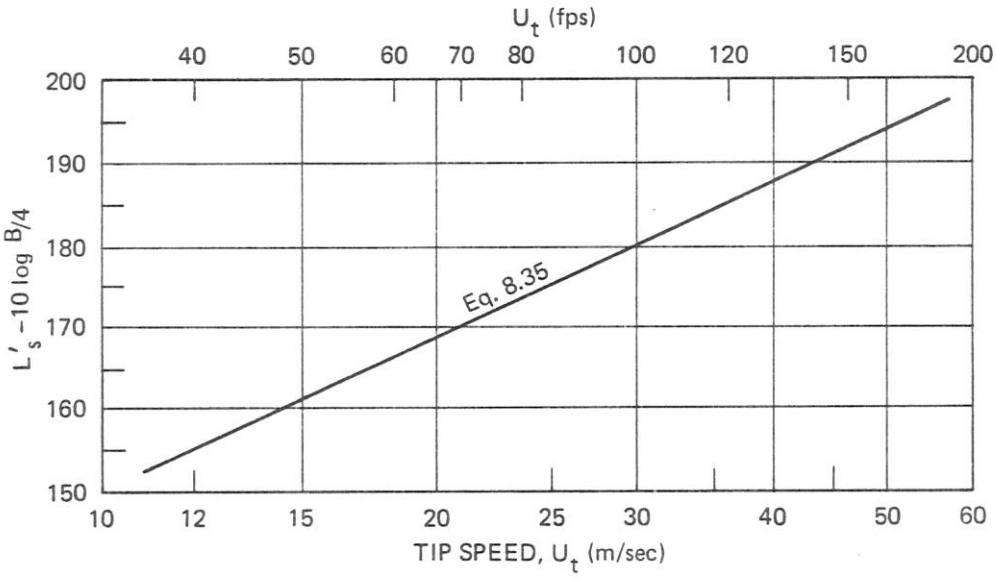

Fig. 8.22. Dependence of Overall Noise Level on Propeller Tip Speed, Based on Data from WWII

Acoustic Efficiencies of Surface Ships

It is instructive to calculate the acoustic conversion efficiency for surface ship propeller cavitation. From Fig. 8.21 and Eq. 8.31, the overall level above 100 Hz for a 12-kt ship of WWII vintage would be about 174 dB re 1μPa, and the overall level for the entire spectrum therefore about 178 dB re 1μPa. This source level implies about 2.5 W acoustic power radiated over a hemisphere. Assuming 3000 hp, the propulsion power would be close to 2.5 MW, resulting in an acoustic conversion efficiency of about 1×10^{-6}. Calculations for a number of specific ships of various types indicate that from 0.3 to 5 W of acoustic power is radiated per MW of mechanical power. Thus, within ±6 dB the acoustic conversion efficiency for propeller cavitation is 1.5×10^{-6}.

Modulation Effects

As discussed in Section 8.4, circumferential wake variations cause strong amplitude modulation effects at blade passage frequency, and slight physical differences between blades produce modulation at the shaft rotational frequency. These modulations give a very distinctive characteristic to surface ship noise and enable experienced sonar operators to classify targets by measuring the turn count and thereby determining propeller rpm.

Shaft and blade modulation frequencies for merchant ships are now significantly higher than they were during WWII. Thirty years ago most merchant ships had three- or four-bladed propellers and operated at from 60 to 100 rpm. Shaft modulation frequencies were generally between 1.0 and 1.6 Hz and blade frequencies were from 3.5 to 6.5 Hz. Today, typical merchant propellers have four, five or six blades and operate at from 75 to 135 rpm; shaft frequencies range from 1.3 to 2.2 Hz, and blade frequencies are typically 6 to 12 Hz.

Tonal Spectra

Dominance of low-frequency spectra by cavitation tonals at multiples of blade-rate frequency, as originally reported by Aleksandrov (1962), has recently been confirmed by Morris (1975) for a supertanker and by unpublished data obtained during a merchant ship noise study conducted under the auspices of the U.S. Naval Oceanographic Office (N.O.O.). Morris measured narrowband spectra from the *CHEVRON LONDON* at ranges of 75 to 250 nautical miles, finding strong tonals at multiples of 6.8 Hz with those from 40 to 70 Hz generally being strongest. Source levels of these tonals were estimated to be as high as 190 dB μPa. Spectrograms obtained during N.O.O.'s measurements of a number of freighters, bulk carriers and tankers also showed strong tonals at multiples of blade frequency, the sixth to ninth harmonics being most prominent. In several instances, high harmonics of shaft-rate frequency were also observed, indicating shaft-rate modulation of blade-frequency tonals.

Merchant Ship Trends

Cargo vessels and tankers that operated during WWII were generally between 90 and 170 m long (300 to 560 ft), displaced less than 20,000 tons and were powered by engines of under 8,000 hp. Ten to 12 kts were typical speeds and propeller tip speeds of 17 to 29 m/sec (55 to 95 fps) were most common. Since most of the world's shipyards had been destroyed, the only new types of ships built during the first decade after the war were a few advanced classes built in the U.S. Beginning in about 1960, as new European and Japanese shipbuilding facilities became available, the process of replacing WWII ships began. Many of these new ships are of sizes and speeds not known before. Previously 15,000 hp delivered to a single shaft had been the maximum; today powers between 32,000 and 42,000 hp per shaft are common. Previously 20,000 tons was considered very large; today many ships exceed 100,000 tons. Previously lengths under 180 m were usual; today lengths of 180 to 370 m (600 to 1200 ft) are typical. The average installed power of all ships at sea has increased from 3000 hp to 9000 hp.

The greatest changes have occurred in oil tankers, bulk carriers and container ships. The most common tankers built in the U.S. during WWII and used for many years afterwards, the T-2 class, were about 160 m (525 ft) long, were rated at about 17,000 deadwt tons, traveled at 14 to 16 kts and were usually powered by 7500 hp turbines. Today's tanker fleet has the capacity of over 20,000 T-2 tankers, a single giant supertanker being equivalent to from 15 to 20 of them. Typical propulsion powers are from 20,000 to 40,000 hp. However, speeds have changed little: 14 to 16 kts is still typical.

Bulk carriers are a relatively new type of ship, built since about 1950. They are similar in construction to oil tankers but are generally intended only for dry bulk cargoes. They are smaller than the largest tankers, two thirds of them being between 15,000 and 70,000 deadwt tons. Bulk carriers and tankers are quite similar in their underwater conformation and therefore have similar acoustic properties. Taken together, tankers and bulk carriers today number over 9000, have a

capacity of nearly 400 million deadwt tons, and are powered by over 100 million hp of propulsion machinery. The two classes account for over 80% of cargo capacity at sea at any one time and about 60% of installed propulsion power.

Containerships are the newest class of merchant ships. These are ships that carry cargo in freight containers stacked on deck. Some are older freighters converted to this purpose; many are especially designed ships built in the last ten years. Most of these newly built ships travel at speeds in excess of 20 kts, a few at over 30 kts. About 50 of the largest ones have multiple propellers and are powered by from 45,000 to 120,000 hp. These are the new queens of the sea, replacing the large passenger liners that have been retired in recent years.

While there are very few underwater noise measurements of modern ships, it seems likely that noise levels have risen significantly from WWII values. Average ship speeds are today about 50% above those of WWII. The trend shown in Fig. 8.21 would predict about a 9 dB rise in the noise radiated by an average ship. Information on typical propeller diameters and rpm's shows that tip speeds are now commonly between 30 and 45 m/sec (100 to 150 fps), about 60% higher than in WWII. In accordance with Eq. 8.35, this increase in tip speed would imply a noise increase of as much as 12 dB. The only mitigating factor might be improvement of the inception index, which could reduce these estimates by 3 to 5 dB. It therefore seems likely that the average noise radiated by individual ships currently at sea is between 5 and 8 dB higher than that common at the end of WWII.

8.7 Ship-Generated Ambient Noise

Recognition of Ships as Sources of Ambient Noise

As discussed in Section 4.4, ambient noise curves developed during WWII were plotted only as a function of sea state and/or wind speed. These curves were intended for use only above 500 Hz since the investigators recognized that ship noise contaminated their low-frequency data. Nevertheless, others extrapolated the curves to lower frequencies and were then surprised when measurements made below 200 Hz showed very little dependence on wind speed or sea state.

During the decade of the 1950's ambient noise measurements were made down to as low as 10 Hz at several deep-water sites in the Atlantic. As reported by Walkinshaw (1960), data above 300 Hz correlated well with wind and weather but levels below about 200 Hz were virtually independent of these factors. Walkinshaw attributed the low-frequency spectrum to noise from distant shipping. In his classic survey article, Wenz (1962) also attributed the non-wind-dependent spectrum in the range of 10 to at least 100 Hz to *traffic noise*, which he defined as noise from distant shipping. The dominance of noise from distant ships has been confirmed by measurements by Axelrod et al (1965) of vertical arrival angles which show that below 200 Hz the major contributions are carried by ray paths that are within 20° of horizontal. Diurnal variations of noise levels at some locations have been attributed to local shipping patterns.

It is now well accepted within the underwater sound community that distant shipping accounts for ambient noise between 20 and 200 Hz in most deep-water, open-ocean areas and in highly traveled seas such as the Baltic and Mediterranean. Only in areas remote from shipping or protected from long-range sounds, such as the South Pacific and southern half of the Indian Ocean, does sea noise dominate throughout the spectrum as represented in Fig. 4.8. Figure 8.23 presents the author's estimate of the shipping contribution to low-frequency ambient noise for four levels of ship noise dependent on the acoustic proximity of shipping.

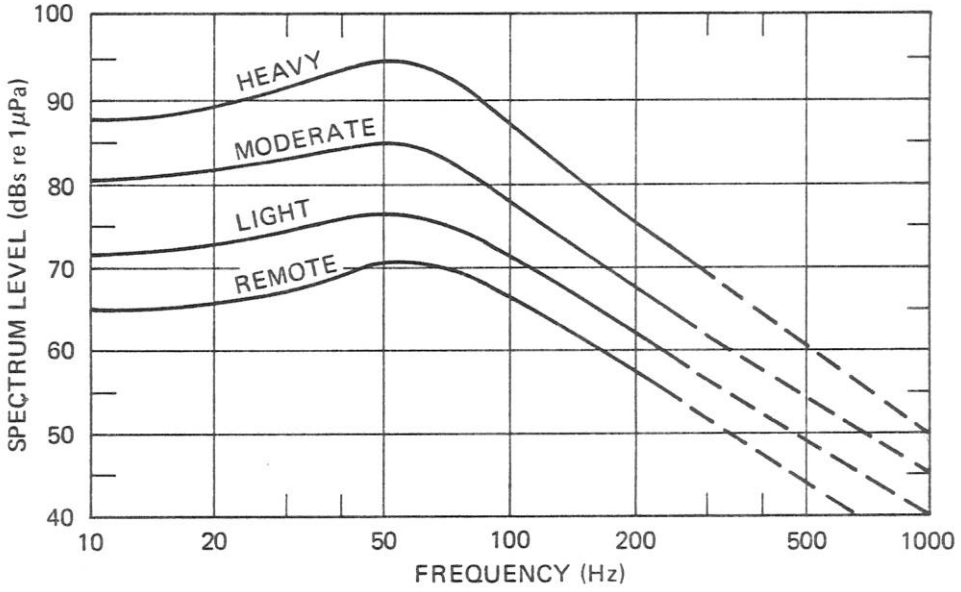

Fig. 8.23. Estimated Spectra Representing Shipping Contribution to Deep-Water Ambient Noise as Function of Shipping Concentration

Reverberant Room Theory of Ambient Noise

Accurate calculation of the contribution of ships to local ambient noise levels requires detailed knowledge of shipping distributions, of long-range sound propagation and of ship spectra. None of these is usually available. Nevertheless, lacking information for detailed calculations, one can derive the salient characteristics of ambient noise originating from ships by treating the ocean as a semi-reverberant volume, much as one would calculate the pressure spectrum from a number of sound sources in room acoustics. The ocean acts like a room in that sound rays change direction at least three times in 100 km because of refractive effects. Reverberant sound will dominate as long as the loss per mean free path is small and there are no dominant sources close to the receiver. These conditions are satisfied in the deep ocean for frequencies below 500 Hz, provided there are no ships closer than about 50 km.

Young (1959) has shown that, when the number of reflections is large, the spatially averaged energy density for steady sources can be expressed by

$$\langle E \rangle = \frac{\overline{p^2}}{\rho_o c_o^2} = \frac{\ell W}{\overline{a} c_o V} , \qquad (8.36)$$

where ℓ is the mean free path between direction reversals, $\overline{a}$ is the mean reflection loss in nepers, W is the source power and V is the total volume of the reverberant space. The volume is the product of the surface area, S, and the effective average water depth, H. The other terms require more explanation. The coefficient, $\overline{a}$, represents the dissipative loss per reflection. In underwater sound, it is more usual to deal with the average attenuation, α, expressed in dB per unit distance. If we

take α_T to include boundary reflection losses as well as volume absorption, then $\overline{a}$ can be related to α_T by

$$\overline{a} = \alpha_T \ell (10 \log e)^{-1} = \frac{\alpha_T \ell}{4.34} , \tag{8.37}$$

where the last factor is required to convert dB into nepers.

Combining Eqs. 8.36 and 8.37 and expressing V by SH, the mean square sound pressure can be related to the average source spectrum of merchant ships by

$$\overline{p^2} = 8.68 \frac{\theta_e \delta}{\alpha_T H} \overline{p_s^2(1)} , \tag{8.38}$$

where δ is the number of ships per unit area and θ_e is a factor incorporated in the analysis to take into account the fact that only rays that radiate in a fairly narrow range of angles near grazing contribute to the reverberant field.

Expressing the ambient sound pressure as a level, L_n, in dB and the average source level per ship by L_s, the ambient level is then related to the source level by

$$L_n = L_s + 10 \log \theta_e - 10 \log \alpha_T H + 10 \log \delta + 9.5 . \tag{8.39}$$

The noise is therefore a function of at least four factors. Equation 8.39 can be better written for order-of-magnitude calculations in terms of ship densities, δ°, expressed in terms of numbers of ships per 1° square. On average, the area of a 1° square is about $10^{10}\,m^2$. Assuming θ_e to be 1/3 radian, Eq. 8.39 becomes

$$L_n \doteq L_s - 95 + 10 \log \delta^\circ + 10 \log \frac{1}{\alpha_T H} . \tag{8.40}$$

This equation serves to explain most observed trends. Thus, the spectral shape of ship-dominated ambient noise should be controlled by the average spectral shape of merchant ships, as modified by frequency dependence of the attenuation term. As reported by Wenz (1962), and more recently by Perrone (1969, 1970, 1974), ambient spectra below 100 Hz do indeed have shapes similar to ship noise spectra shown in Fig. 8.20. Above 100 Hz the shipping contribution decreases somewhat faster than that shown in Fig. 8.20 due to increased absorption. Equation 8.40 also explains geographical variations and long-term trends and forms a basis for understanding spatial and temporal fluctuations.

Geographical Variations

Figure 8.23 reveals about 25 dB variation in traffic noise between areas remote from shipping and those near busy shipping lanes. While the average ship density over all ocean areas is estimated to be about 0.4 ships per 1° square, the number varies from as low as 0.02 in the South Pacific and other remote areas to over 1 for the North Atlantic and as high as 5 to 10 near the coast of Europe. Thus, this factor alone can account for as much as 25 dB of geographical variability.

Propagation differences can also account for 5 to 10 dB differences in shipping noise. In some

areas, sound transmission is primarily by refractive paths that do not interact directly with the surface or bottom. In such cases, α_T equals that due to volume absorption alone, for which a value of 0.2 dB per 100 km is representative. Assuming an ocean depth of 4 km, the term involving $\alpha_T H$ would add 20 dB. On the other hand, if the water depth is not sufficient to support refractive transmission, losses will occur at each bottom and surface interaction. Experimental data for this type of propagation generally show between 0.05 and 0.2 dB loss relative to cylindrical spreading in a distance equal to the water depth, giving an average value of the transmission term in Eq. 8.40 of only about 10 dB and resulting in lower ambient levels for the same shipping density.

Importance of Coastal Shipping

Even at locations remote from the edges of an ocean basin, low-frequency ambient noise is often dominated by coastal shipping. The reason is that sound propagates especially well from sources located in relatively shallow water at the edge of a deep basin. As the sound rays propagate seaward, each bounce from the sloping bottom reduces the angle by twice the bottom slope angle. Rays that would otherwise interact with the bottom and/or surface become deep channel rays that propagate with minimum loss. This is equivalent both to increasing the angle θ_e and to assuring that propagation occurs with minimum α_T.

The existence of the *coastal region enhancement effect* was demonstrated by Northrop et al (1968) using explosive charges. They found that sounds from such charges exploded off the California coast were received by deep hydrophones over 3000 miles away at a level at least 15 dB higher than that from similar sources over a flat bottom. Since the slope acts to channel the sound, Smith (1971) termed it the *megaphone effect*. A more complete explanation showing the importance of the bigradient sound-speed profile in channeling the sound was given by Smith and Jones (1972). More recently, Morris (1975) found that levels received when a supertanker proceeded toward port were enhanced 3 to 6 dB as it neared the coast. Other measurements show 6 to 10 dB to be more typical.

Directional Characteristics

The sound field in a truly reverberant room does not exhibit directional characteristics. However, the ocean is more like a long, highly-reverberant hallway than a room. Since shipping distributions are not uniform, and propagation is often more favorable in some directions than others, ambient noise at low frequencies may be expected to exhibit horizontal directionality of at least several dB and in many cases of more than 10 dB. This is very much a local effect dependent on location of ships at basin edges as well as on depth of the receiver and on sound velocity profile. Its calculation requires detailed knowledge of shipping distribution as well as sound propagation.

Vertical directionality depends somewhat on receiver depth and type of propagation. However, low-frequency ambient noise normally arrives within ±20° of horizontal.

Temporal Fluctuations

Transmission from near-surface sources to distant receivers is very much a function of the speed of sound at the surface relative to that near the bottom. If the sound speed is lower at the surface, sound can be transmitted without bottom interaction; if it is higher, all rays may strike the bottom. As discussed earlier in this section, the difference in the effective value of the absorption coefficient in these two cases is often of the order of a factor of 10, resulting in 10 dB difference in low-frequency ambient levels. There are many places where the warming of the

surface waters in summer is sufficient to change refractive transmission to bottom interacting transmission. In these areas, seasonal variations of ambient noise may be expected to exceed 5 dB.

Wenz (1972) reported diurnal fluctuation at a number of coastal locations. This is probably due more to changes in nearby shipping patterns than to distant shipping effects. Port arrival and departure times tend to cluster around certain hours, which could cause peaking of local traffic interference at any coastal location close to a busy port. Wenz found that diurnal fluctuation may be only a dB or two in remote areas, but that 5 to 6 dB is quite common for coastal locales, and that in some locations, such as that illustrated by Fig. 8.24, fluctuation due to local shipping regularly exceeds 20 dB.

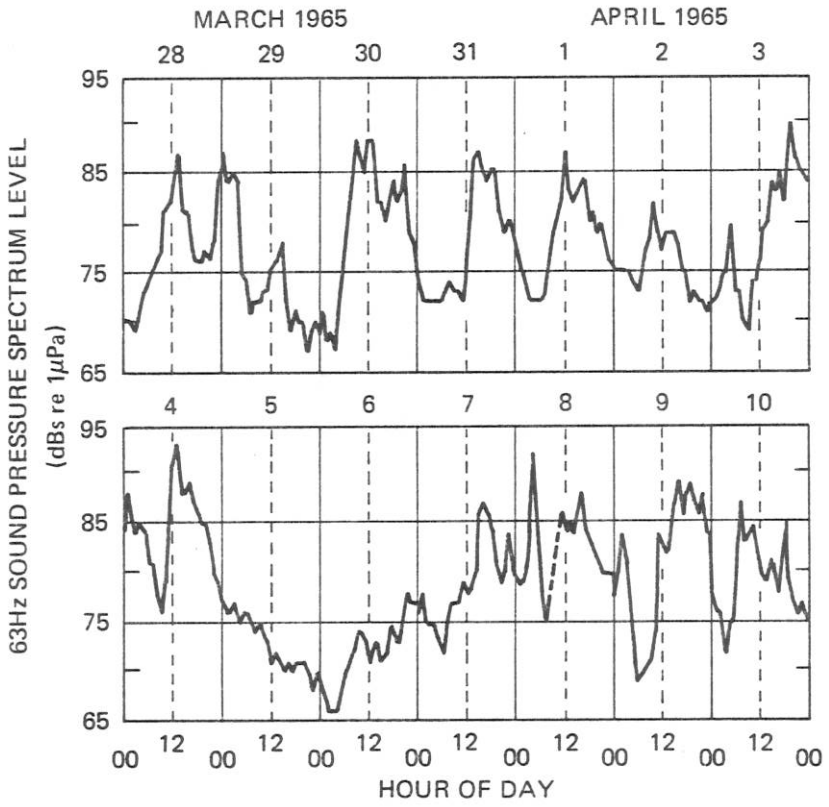

Fig. 8.24. Fluctuations of Low-Frequency Ambient Noise at a Coastal Location, from Wenz (1972)

In addition to seasonal effects due to changes of the surface sound speed and diurnal effects due to local ship patterns, there are short-term fluctuations. These are of the order of minutes and are analogous to the scintillation of starlight. Transmission of sound is itself a fluctuating phenomenon, variations occurring with both time and position. As individual ships move across the ocean surface, they move into and out of regions of exceptionally good transmission. Dyer (1970, 1973) showed that the standard deviation for multipath transmission is of the order of 5 dB, and that the value for ship-generated ambient noise depends on the density of shipping, array beam width and analysis frequency band. Typical values of the standard deviation when

measuring with omnidirectional phones and one-third-octave bandwidths are 1.5 to 2.5 dB for the distant shipping component alone. When data are contaminated by nearby ships, as in Fig. 8.24, standard deviations are much larger.

It is common practice in the underwater sound community to assume a log-normal distribution of ambient noise values. While this offers a reasonable fit to the central distribution, a Gaussian function does not properly represent the tails. Dyer (1973) concluded that the actual distribution is closer to a Rayleigh distribution, which is similar to Gaussian but with truncated tails.

Long-Term Trends

One of the more important conclusions that follows from this analysis of shipping noise is that low-frequency ambient noise levels must have risen significantly in the past quarter century. In the 25 years following 1950, the total number of ships has more than doubled. With increased efficiencies of port handling facilities, the number of ships at sea has increased even more. This factor alone would account for a 3 to 5 dB increase of ambient noise originating from shipping. In addition, as discussed in the previous section, increases of average ship speed, propulsion power and propeller tip speed all lead to the conclusion that the average ship produces at least 6 dB more noise. Combining all these factors, one must conclude that in the past 25 years ambient noise has probably risen about 10 dB in those areas where shipping noise dominates. Furthermore, ship noise must now have become a dominant factor in some areas where it did not previously control. Unfortunately, measurements made at the same location a decade or more apart have not appeared in the literature, so this conclusion cannot be supported with experimental data. However, in view of the nearly tenfold increase of the horsepower of propulsion plants in ships at sea, it would indeed be remarkable if the noise due to ships had not increased close to 10 dB.

This trend is not expected to continue at so rapid a pace. Over the next 25 years, the number of ships may be expected to increase only about 50%, and the noise per ship by only a few dB. Thus, the increase of low-frequency ambient noise levels due to ships may be only about 5 dB during the next quarter century.

REFERENCES

Sections 8.1-8.4

Aleksandrov, I.A., Some cavitation characteristics of ship propellers, *Sov. Phys.-Acoustics, 7*, 67-69, 1961.

Aleksandrov, I.A., Physical nature of the rotation noise of ship propellers in the presence of cavitation, *Sov. Phys.-Acoustics, 8*, 23-28, 1962.

Boswell, R.J., Design, Cavitation Performance, and Open-Water Performance of a Series of Research Skewed Propellers, *N.S.R.D.C. Rept. 3339*, March 1971 (AD 732511).

Burrill, L.C., Sir Charles Parsons and cavitation, *Trans. Inst. Mar. Engin., 63*, 149-167, 1951.

Burrill, L.C., The phenomenon of cavitation, *Int. Shipbuilding Progress, 2*, 503-511, 1955.

Burrill, L.C. and Emerson, A., Propeller cavitation: tests on 16-inch models in the King's College cavitation tunnel, *Northeast Coast. Inst. Engin. and Shipbuilders, 70*, 121, 1953; also, *Int. Shipbuilding Progress, 10*, 119-131, 1963.

Eisenberg, P., On the Mechanism and Prevention of Cavitation, *D.T.M.B. Rept. 712*, July 1950.

Emerson, A. and Sinclair, L., Propeller cavitation: systematic series tests on 5- and 6-bladed model propellers, *Trans. Soc. Naval Arch. and Mar. Engin., 75*, 224-267, 1967.

Flamm, O., The scientific study of naval architecture in Germany, *Trans. Inst. of Naval Arch., 53*, 207-216, 1911.

Goldstein, S., On the vortex theory of screw propellers, *Proc. Roy. Soc. (London), A123*, 440-465, 1929.

Huse, E., Propeller-hull-vortex cavitation, *Int. Shipbuilding Progress, 19*, 111-125, 1972.

Lane, F., Optimum single propellers in radially varying, incompressible inflow, *J. Appl. Mech., 19*, 252-256, 1952.

Lerbs, H.W., "On the Development of the Theory of Marine Propulsion," Paper 7 of *Symposium on Naval Hydrodynamics*, Nat. Acad. of Sciences, Nat. Res. Council Publ. 515, Washington, 1956 (pp. 155-179).

Lesunovskii, V.P. and Khokha, Yu V., Characteristics of the noise spectrum of hydrodynamic cavitation on rotating bars in water, *Sov. Phys.-Acoustics, 14*, 474-478, 1968.

McCormick, B.W., Jr., Eisenhuth, J.J. and Lynn, J.E., A Study of Torpedo Propellers - Part 1, Theory, *Ord. Res. Lab. Rept. 16597-5*, March 1956.

Mellen, R.H., Ultrasonic spectrum of cavitation noise in water, *J.A.S.A., 26*, 356-362, 1954.

Morgan, W.B. and Lichtman, J.Z., "Cavitation Effects on Marine Devices," in *Cavitation State of Knowledge*, A.S.M.E., 1969 (pp. 195-241).

Robertson, J.M., Water tunnels for hydraulic investigations, *Trans. A.S.M.E., 78*, 95-104, 1956.

Ross, D. and McCormick, B.W., Jr., "Effect of Air Content on Cavitation Noise," report to *Eighth American Towing Tank Conference*, Oct. 1948; also, A Study of Propeller Blade-Surface Cavitation Noise, *Ord. Res. Lab. Rept. 7958-115*, Oct. 1948.

Theodorsen, T., *Theory of Propellers*, McGraw-Hill, New York, 1948.

Van de Voorde, C.B., A full scale model correlation investigation on propeller cavitation, *Int. Shipbuilding Progress, 8*, 255-266, 1961.

van Gent, W. and van Oossanen, P., Influence of wake on propeller loading and cavitation, *Int. Shipbuilding Progress, 20*, 279-321, 1973.

van Manen, J.D., The effect of cavitation on the interaction between propeller and ship's hull, *Int. Shipbuilding Progress, 19*, 3-20, 1972.

van Oossanen, P., A method for minimizing the occurrence of cavitation on propellers in a wake, *Int. Shipbuilding Progress, 18*, 321-333, 1971.

von Mises, R., *Theory of Flight*, McGraw-Hill, New York, 1945 (Chapters 11 and 12).

Sections 8.5 and 8.6

Dorman, W.J. and de Koff, D.L., Characteristics of recent large container ship designs, *Marine Technology, 8*, 453-464, 1971.

Dow, M.T., Emling, J.W., Knudsen, V.O., "Survey of Underwater Sound; Report No. 4, Sounds from Surface Ships," *O.S.R.D., Div. 6.1, N.D.R.C. Rept.*, June 1945 (Declassified Aug. 1960).

Kopec, B.M., The ships of the US-flag intermodal fleet, *Proc. U.S. Naval Inst., 101*, No. 5, 213-230, 1975.

Knudsen, V.O., Alford, R.S. and Emling, J.W., "Survey of Underwater Sound; Report No. 2, Sounds from Submarines," *O.S.R.D., Div. 6.1, N.D.R.C. Rept.*, 1943 (Declassified).

Morris, G.B., Preliminary Results on Seamount and Continental Slope Reflection Enhancement of Shipping Noise, *Marine Phys. Lab. Rept. SIO Ref. 75-34*, Nov. 1975.

"Principles and Applications of Underwater Sound," Vol. *7, Summary Tech. Rept. of Div. 6, N.D.R.C.*, 1946 (Chapter 12).

Ross, D., Trends in Merchant Shipping (1969-1980), *Tetra Tech, Inc. Rept. SD-449-75-1*, April 1975.

Strasberg, M. and Sette, W.J., Measurements of Propeller Noise on Three Submarines of the SS 212 Class, *D.T.M.B. Rept. R-205*, 1944.

Urick, R.J., *Principles of Underwater Sound for Engineers*, McGraw-Hill, New York, 1967 (Chapter 10).

Jane's Flighting Ships.

Jane's Freight Containers.

Lloyd's Register of Shipping, Statistical Tables, pub. annually.

"A Statistical Analysis of the World's Merchant Fleets," publ. annually by the U.S. Dept. of Commerce, Maritime Administration.

"Acoustic Torpedoes," Vol. *22, Summary Tech. Rept. of Div. 6, N.D.R.C.*, 1946 (Section 3.2).

Section 8.7

Axelrod, E.H., Schoomer, B.A. and Von Winkle, W.A., Vertical directionality of ambient noise in the deep ocean at a site near Bermuda, *J.A.S.A., 37*, 77-83, 1965.

Arase, E.M. and Arase, T., Correlation of ambient sea noise, *J.A.S.A., 40*, 205-210, 1966.

Arase, E.M. and Arase, T., Ambient sea noise in the deep and shallow ocean, *J.A.S.A., 42*, 73-77, 1967.

Dyer, I., Statistics of sound propagation in the ocean, *J.A.S.A., 48*, 337-345, 1970.

Dyer, I., Statistics of distant shipping noise, *J.A.S.A., 53*, 564-570, 1973.

Frosch, R.A., How to make an ambient noise in the ocean, Paper C1, 59th Meeting A.S.A., *J.A.S.A., 32*, 915, 1960; also, *Hudson Labs. Contrib. 81*, 1960.

Knudsen, V.O., Alford, R.S. and Emling, J.W., "Survey of Underwater Sound; Report No. 3, Ambient Noise," *O.S.R.D., Div. 6.1, N.D.R.C. Rept. 1848*, 1944.

Morris, G.B., *op cit.*

Northrop, J., Loughridge, M.S. and Werner, E.W., Effect of near-source bottom conditions on long-range sound propagation in the ocean, *J. Geophys. Res., 73*, 3905-3908, 1968.

Perrone, A.J., Deep-ocean ambient noise spectra in the northwest Atlantic, *J.A.S.A., 46*, 762-770, 1969.

Perrone, A.J., Ambient noise spectrum level as function of water depth, *J.A.S.A., 48*, 362-370, 1970.

Perrone, A.J., Infrasonic and low-frequency ambient noise measurements on the Grand Banks, *J.A.S.A., 55*, 754-758, 1974.

Smith, P.W., Jr., Sound transmission in isogradient shallow water over a plane sloping bottom, Paper Q2, 80th Meeting A.S.A., *J.A.S.A., 49*, 96, 1971.

Smith, P.W., Jr. and Jones, J.P., Transmission into a basin having a bigradient sound-speed profile, Paper M5, 83rd Meeting A.S.A., *J.A.S.A., 52*, 137, 1972.

Talham, R.J., Ambient-sea-noise model, *J.A.S.A., 36*, 1541-1544, 1964.

Walkinshaw, H.M., Low-frequency spectrum of deep ocean ambient noise, Paper D1, 60th Meeting A.S.A., *J.A.S.A., 32*, 1497, 1960.

Wenz, G.M., Acoustic ambient noise in the ocean: spectra and sources, *J.A.S.A., 34*, 1936-1956, 1962.

Wenz, G.M., Review of underwater acoustics: noise, *J.A.S.A., 51*, 1010-1024, 1972.

Young, R.W., Sabine reverberation equation and sound power calculations, *J.A.S.A., 31*, 912-921, 1959.